Inorganic Chemistry

Article

pubs.acs.org/IC

Fluorescent Zinc Sensor with Minimized Proton-Induced Interferences: Photophysical Mechanism for Fluorescence Turn-On Response and Detection of Endogenous Free Zinc Ions

Ji Eon Kwon,[†,⊥] Sumin Lee,[‡,⊥] Youngmin You,*[,‡] Kyung-Hwa Baek,[§] Kei Ohkubo,[∥] Jaeheung Cho,[‡] Shunichi Fukuzumi,*[,‡,∥] Injae Shin,*[,§] Soo Young Park,*[,†] and Wonwoo Nam*[,‡]

[†]Department of Materials Science & Engineering, Seoul National University, San 56-1, Sillim 9-dong, Gwanak-gu, Seoul 151-744, Korea

[‡]Department of Bioinspired Science, Ewha Womans University, Daehyun-dong, Seodaemun-gu, Seoul 120-750, Korea

[§]Department of Chemistry, Yonsei University, Sinchon-dong, Seodaemun-gu, Seoul 120-749, Korea

[∥]Department of Material and Life Science, Graduate School of Engineering, Osaka University, ALCA, Japan Science and Technology Agency (JST), Suita, Osaka 565-0871, Japan

Supporting Information

ABSTRACT: A new fluorescent zinc sensor (HNBO−DPA) consisting of 2-(2′-hydroxy-3′-naphthyl)benzoxazole (HNBO) chromophore and a di(2-picolyl)amine (DPA) metal chelator has been prepared and examined for zinc bioimaging. The probe exhibits zinc-induced fluorescence turn-on without any spectral shifts. Its crystal structure reveals that HNBO−DPA binds a zinc ion in a pentacoordinative fashion through the DPA and HNBO moieties. Steady-state photophysical studies establish zinc-induced deprotonation of the HNBO group. Nanosecond and femtosecond laser flash photolysis and electrochemical measurements provide evidence for zinc-induced modulation of photoinduced electron transfer (PeT) from DPA to HNBO. Thus, the zinc-responsive fluorescence turn-on is attributed to suppression of PeT exerted by deprotonation of HNBO and occupation of the electron pair of DPA, a conclusion that is further supported by density functional theory and time-dependent density functional theory (DFT/TD-DFT) calculations. Under physiological conditions (pH 7.0), the probe displays a 44-fold fluorescence turn-on in response to zinc ions with a K_d value of 12 pM. The fluorescent response of the probe to zinc ions is conserved over a broad pH range with its excellent selectivity for zinc ions among biologically relevant metal ions. In particular, its sensing ability is not altered by divalent transition metal ions such as Fe(II), Cu(II), Cd(II), and Hg(II). Cell experiments using HNBO−DPA show its suitability for monitoring intracellular zinc ions. We have also demonstrated applicability of the probe to visualize intact zinc ions released from cells that undergo apoptosis. More interestingly, zinc-rich pools in zebrafish embryos are traced with HNBO−DPA during early developmental stages. The results obtained from the *in vitro* and *in vivo* imaging studies demonstrate the practical usefulness of the probe to detect zinc ions.

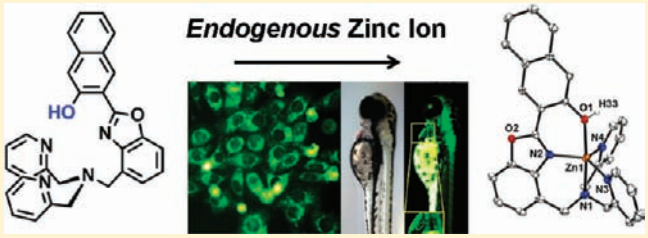

I. INTRODUCTION

Zinc ion is the second abundant transition metal ion in the human body (2−3 g in total), and it plays diverse roles in human physiopathology.[1−5] While total zinc concentrations are high, concentrations of *free zinc ions* that are loosely bound to proteins are relatively low[6−8] and tightly regulated.[9−14] Recent studies have associated failures in homeostasis of free zinc ions with neurological diseases such as Alzheimer's disease, amyotrophic lateral sclerosis (ALS), Parkinson's disease, ischemia, and epilepsy.[15−17] In addition, free zinc ions are also involved in regulation of programmed cell death (i.e., apoptosis).[18−20] Thus, a sensitive and noninvasive technique to trace and visualize free zinc ions would be highly demanded. Since the zinc ion itself is spectroscopically silent due to its $3d^{10}$ electron configuration, the development of highly sensitive and selective fluorescent sensors for zinc ions is therefore of critical importance.[21−28]

Much effort has been devoted to the development of fluorescent zinc sensors to detect endogenous free zinc ions.[28−33] A typical structure of a fluorescent zinc sensor is a conjugate composed of a fluorophore and a zinc-specific receptor such as di(2-picolyl)amine (DPA), *N*,*N*-di(2-picolyl)-ethylenediamine (DPEN), tris(2-picolyl)amine (TPA), or *N*,*N*,*N*′-tris(2-picolyl)ethylenediamine (TRPEN).[21] In the zinc-free form, these receptors transfer their electron to the adjacent fluorophores in the excited state, partially quenching the fluorescence emission, whereas the nonradiative electron

Received: March 2, 2012
Published: April 25, 2012

   dx.doi.org/10.1021/ic300476e | *Inorg. Chem.* 2012, 51, 8760−8774

Scheme 1. Synthesis of the Fluorescent Zinc Sensor HNBO−DPA

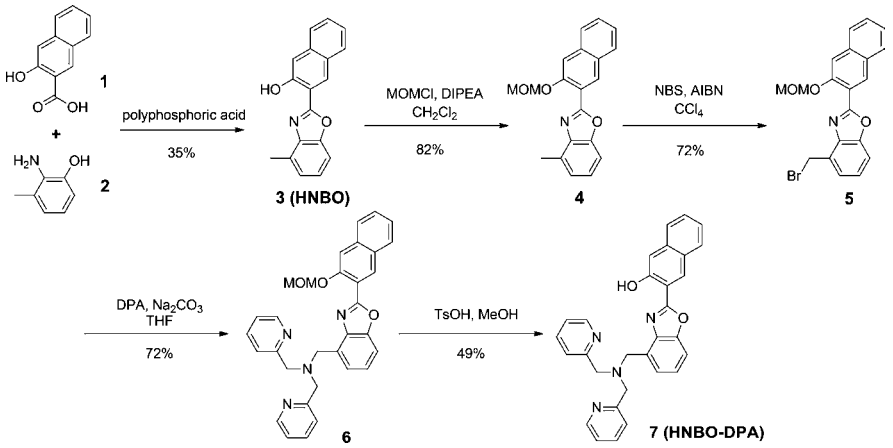

transfer is suppressed when a zinc ion is coordinated and the emission is consequently strong. This modulation in photoinduced electron transfer (PeT) thus allows zinc detection by means of fluorescence turn-on. The success of PeT-based sensors has promoted extensive variations of molecular structures,[31] which aim at improved zinc selectivity and optimized dissociation constant (K_d).[34−40] Structural changes in receptors, however, always perturb oxidation potentials, affecting the modulation of the PeT process. Moreover, protonation of the zinc receptors produces false positive signals.[25] Fluorescent sensors based on intramolecular charge transfer (ICT) also suffer from pH dependence.[41,42] Thus, the capability of fluorescent detection by the modulation of electron transfer is limited. To circumvent this problem, approaches taking advantage of a variety of signaling mechanisms other than electron transfer have been developed, such as twisted intramolecular charge transfer (TICT),[43] fluorescence resonance energy transfer (FRET),[44] and excimer formation.[45] These mechanisms are, however, governed by intramolecular torsional or intermolecular translational motions which are indirect consequences of zinc coordination.

Excited-state intramolecular proton transfer (ESIPT) is characteristic of molecules that possess an intramolecular hydrogen bond between a proton−donor moiety (i.e., −OH) and a proton−acceptor moiety (i.e., −N═) in a five- or a six-membered ring, with tautomerization occurring upon photoexcitation. The photoinduced tautomerization transiently generates a keto form (i.e., ═O and −NH−), which typically produces fluorescence with a large Stokes shift (6000−12 000 cm^{-1}). Reverse proton transfer in the ground state from the keto form (K) to the enol form (E) completes a four-level cyclic proton transfer reaction (E → E* → K* → K → E).[46,47] Suppression of ESIPT results in enol fluorescence that is hypsochromically shifted compared to the keto fluorescence.[48−50] Fluorescence ratiometric sensing can be therefore accomplished because metal coordination prohibits ESIPT. This attractive sensing mechanism indeed promoted development of a number of fluorescent zinc sensors, but most of them were studied only in organic solutions.[51−55]

The ESIPT process is, however, inhibited in aqueous solution due to strong hydrogen bonding interactions with water, and normal enol fluorescence thus dominates. In addition, the proton undergoing ESIPT is lost at high pH or in the presence of competing Lewis acids such as biological metal ions. Fahrni and co-workers established the aqueous solution properties of 2-(sulfoamidophenyl)benzimidazole derivatives and reported convincing evidence that zinc displaces the ESIPT amido proton.[56,57] To the best of our knowledge, there is only one report on zinc bioimaging using an ESIPT-based sensor. O'Halloran and co-workers achieved two-photon fluorescence zinc imaging using a sensor (Zinbo-5) based on an ESIPT chromophore, 2-(2′-hydroxyphenyl)benzoxazole.[58] However, mechanistic investigations of its fluorescent response to zinc ions remain elusive. Despite the limited studies to date, metal sensors based on ESIPT chromophores are attractive because the direct interaction of a metal ion with an ESIPT center should allow for facile controls in fluorescence properties. Moreover, well-established photophysics and a large structural library can contribute to a significantly broadened class of bioimaging probes. It is notable that ESIPT platforms have a striking structural analogy to clioquinol that inhibits β-amyloid accumulation during the development of Alzheimer's disease.[59] Therefore, study on elucidation of photophysical processes and biological utilities of ESIPT platforms is of great importance for biomedical studies.

Herein, we report a new fluorescent zinc sensor (HNBO−DPA) that is constructed based on an ESIPT fluorophore, 2-(2′-hydroxy-3′-naphthyl)benzoxazole (HNBO). A zinc-selective di(2-picolyl)amino (DPA) receptor[60−62] is tethered to HNBO through a methylene linker. Fluorescence turn-on response to zinc ions is rationalized through extensive mechanistic studies, including quantum chemical calculations, electrochemical measurements, steady-state spectroscopy, and femtosecond and nanosecond laser flash photolysis experiments. The studies establish a novel fluorescence turn-on principle that is free from detrimental proton-induced background interferences. The zinc sensing capability has been thoroughly assessed under physiological conditions and has been shown to be excellent for detection of biological free zinc ions. It has been demonstrated that the probe can be used to visualize endogenous zinc ions of apoptotic cells and zebrafish embryos. It is expected that the complete research reported in this paper will provide important guidance to future development of ESIPT-based probes for bioimaging applications.

II. RESULTS AND DISCUSSION

Synthesis of the Zinc Sensor. The fluorescent zinc sensor (HNBO−DPA) consists of two functional units, a zinc-specific di(2-picolyl)amino (DPA) receptor and a chromophoric unit (HNBO) featuring ESIPT fluorescence (Scheme 1). The

dx.doi.org/10.1021/ic300476e | Inorg. Chem. 2012, 51, 8760−8774

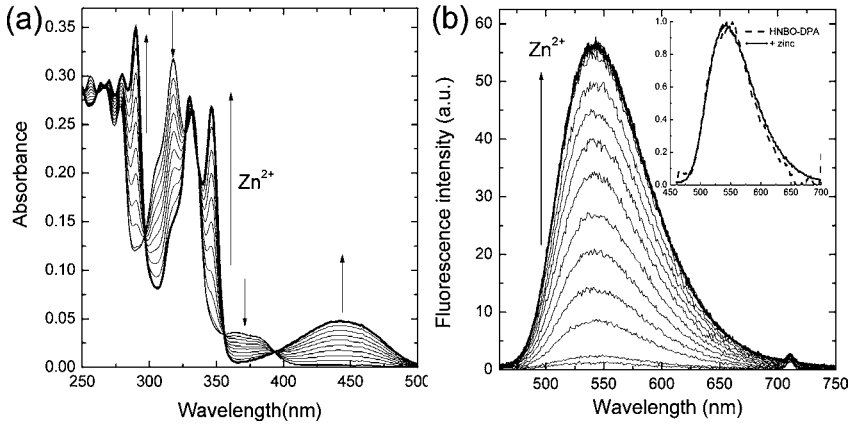

Figure 1. Zinc titration of HNBO−DPA (10 μM in CH_3CN, room temperature). (a) UV−vis absorption spectral change with the continuous addition of $Zn(ClO_4)_2$ (0−1.2 equiv). (b) Fluorescence spectral change with the continuous addition of $Zn(ClO_4)_2$ (0−5 equiv). λ_{ex} = 360 nm. (inset) Normalized fluorescence spectra in the absence (dashed line) and presence (solid line) of zinc ions (5 equiv). Refer to the Supporting Information for corresponding titration isotherms.

structure is reminiscent of Zinbo-5 established by O'Halloran and co-workers,[58] but red-shifted fluorescence is expected due to increased conjugation by naphthol. We anticipated tight zinc binding by the cooperative chelation of naphthol and benzoxazole of HNBO as well as the DPA unit. HNBO−DPA was prepared in five steps with an overall yield of 7%, as shown in Scheme 1. Acid-catalyzed condensation between 2-amino-*m*-cresol and 2-hydroxy-3-naphthoic acid yielded the ESIPT unit (**3**, HNBO), followed by protection of the naphthol group by conversion to a methoxymethylether (MOM). The methyl group of the MOM-protected HNBO (**4**) was brominated with *N*-bromosuccinimide (NBS) and azobisbutyronitrile (AIBN) to benzyl bromide, which was then substituted by DPA in the presence of sodium carbonate. Finally, the MOM group was deprotected by *p*-toluenesulfonic acid (TsOH). HNBO−DPA exhibited excellent solubility in various organic solvents and aqueous buffer solutions (pH 7.0). HNBO−DPA and newly synthesized compounds were characterized by standard analytical methods and proved to be identical with the anticipated structures (see Experimental Section).

Fluorescent Zinc Response. Addition of $Zn(ClO_4)_2$ to an CH_3CN solution of HNBO−DPA (10 μM) immediately turned the colorless solution to yellow due to a new absorption band at 443 nm. A similar observation was reported for the zinc binding of 2-(sulfoamidophenyl)benzimidazole.[56] UV−vis absorption spectra were acquired with continuous addition of zinc ions, and isosbestic points were observed at 261, 297, 327, 336, 355, and 392 nm (Figure 1a). Titration isotherms plotting absorbance at 364 and 443 nm as a function of amount of added zinc ions (0−1.2 equiv) indicate a 1:1 binding stoichiometry (Supporting Information (SI), Figure S1a). Acquisition of photoluminescence spectra (λ_{ex} = 360 nm) of an CH_3CN solution of HNBO−DPA (10 μM) with continuous addition of $Zn(ClO_4)_2$ (0−5 equiv) revealed a 37-fold fluorescence turn-on without a spectral shift (Figure 1b). Actually, normalized photoluminescence spectra of zinc-free and -bound forms are identical (inset of Figure 1b). The lack of a spectral shift is indicative of a fluorescence transition from an identical excited state regardless of the presence of zinc ions, which seems to contradict to the ratiometric change in the UV−vis absorption spectra (Figure 1a). A titration isotherm constructed by total fluorescence intensity as a function of the amount of added zinc ions confirms the 1:1 complexation (SI, Figure S1b).

Table 1. Photophysical and Electrochemical Data of HNBO−DPA in the Absence and Presence of Zinc Ions[a]

	zinc-free	zinc-bound
λ_{abs} (nm, log ε)	318 (4.50), 332 (4.42), 365 (3.56), 379 (3.51)	290 (4.55), 330 (4.45), 346 (4.43), 443 (3.67)
λ_{ems} (nm)[b]	550	542
Φ_{Fl} (%)	0.59	16
brightness ($\varepsilon_{340\ nm} \times \Phi_{Fl}$)	106	3040
τ_{obs} (ns)[c]	20	22
k_r ($/10^7\ s^{-1}$)[d]	0.00295	0.727
k_{nr} ($/10^7\ s^{-1}$)[e]	4.97	3.82
E_p (Ox)[f]	1.11, 1.62	1.50

[a] 10 μM HNBO−DPA in CH_3CN. [b] λ_{ex} = 340 nm. [c] λ_{obs} = 540 nm. [d] $k_r = \Phi_{Fl}/\tau_{obs}$. [e] $k_{nr} = (1 - \Phi_{Fl})/\tau_{obs}$. [f] Determined by cyclic voltammetry (vs SCE); Pt wire working and counter electrodes; An $Ag/AgNO_3$ pseudoreference electrode; 0.1 M Bu_4NPF_6; 1 mM HNBO−DPA; scan rate = 100 mV/s.

In order to elucidate the zinc binding mode of HNBO−DPA, crystals were grown by layering an CH_3CN solution of 1 mM $Zn(ClO_4)_2$ on top of an CH_3CN solution of 1 mM HNBO−DPA (crystallographic data are summarized in SI, Table S1). As shown in Figure 2, the crystal structure reveals that a zinc ion is pentacoordinatively bound to HNBO−DPA through the interactions with the DPA and the ESIPT moiety of HNBO. Thus, the coordination structure around the zinc center is a distorted trigonal bipyramidal. Therefore, it is likely that the tight zinc binding leads to direct alteration of fluorescence properties of HNBO, which is beneficial for detection of trace amount of free zinc ions.

It is worth noting that the photoluminescence response of HNBO−DPA is different from the usual scheme of the ESIPT process that contains the enol to keto tautomerization. This observation is rather in sharp contrast to previous ESIPT sensors that display ratiometric responses.[63−71] In previous cases, zinc ion displaces proton and suppresses the ESIPT process. Hypsochromically shifted fluorescence is therefore observed,[72−74] producing ratiometric signals. The zinc-induced fluorescence enhancement and lack of the fluorescence

dx.doi.org/10.1021/ic300476e | Inorg. Chem. 2012, 51, 8760−8774

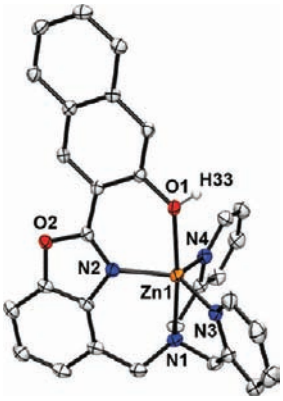

Figure 2. X-ray crystal structure of $[Zn(HNBO–DPA)]^{2+}$ with thermal ellipsoids drawn at the 50% probability level. Hydrogen atoms except H33 are omitted for clarity. H33 atom is found from Fourier difference map. Selected bond distances: Zn1–O1, 2.1877(12) Å; Zn1–N1, 2.1800(14) Å; Zn1–N2, 1.9932(14) Å; Zn1–N3, 2.0169(14) Å; Zn1–N4, 2.0214(15) Å. A list of metric parameters is summarized in SI, Table S2.

ratiometric response observed in our case is, thus, quite unusual. We notice that, despite their ambitious and broad prospects for bioimaging applications, photophysical and electrochemical interactions between a metal-chelating unit and an ESIPT chromophore have been poorly understood to date. This prompted us to elucidate the photophysical origin of the fluorescence response of HNBO–DPA.

Steady-State Photophysics. Fluorescence spectra of HNBO and HNBO–DPA were acquired in various solvents with different polarities. Fluorescence spectra of HNBO are characterized by dual emission that consists of enol (420 nm; Stokes shift = 5600 cm^{-1}) and keto (~650 nm; Stokes shift = ca. 14 000 cm^{-1}) fluorescence (Figure 3a). The enol fluorescence displays a negligible shift by solvent polarity in contrast to the keto fluorescence that shows strong positive solvatochromism.[75] The fluorescence intensity ratio between keto vs enol emission decreases upon increasing solvent polarity. Nevertheless, the dual (enol and keto) fluorescence was observed in all cases. In sharp contrast, HNBO–DPA has an additional emission band (519–554 nm; Stokes shift = 11 000–10 000 cm^{-1}) that occurs between enol and keto fluorescence, producing peculiar *triple* emission (Figure 3b). Fluorescence intensity of this new emission is the strongest among the three emission bands in most organic solvents, and its peak wavelength is significantly affected by solvent polarity. Actually, a bathochromic shift is observed with increasing solvent polarity. This positive solvatochromism is further confirmed by a negative slope (−7662 cm^{-1}) in a Lippert–Mataga plot shown in Figure 3c. Charge-transfer is therefore involved appreciably in the fluorescence transition. Collectively, the spectral position and strong solvatochromism reveal that an origin of the new fluorescence emission is neither enol nor keto state.

Addition of an aqueous sodium hydroxide solution (50 equiv) to CH_3CN solutions containing either HNBO or HNBO–DPA (10 μM) produces a new absorption band at 425 nm (HNBO; Figure 4a) or 433 nm (HNBO–DPA; Figure 4c), respectively. It should be noted that these absorption bands are similar to the case produced by zinc coordination of HNBO–DPA (Figure 1a). The absorption change accompanies a concurrent increase in fluorescence intensity at 560 and 554 nm

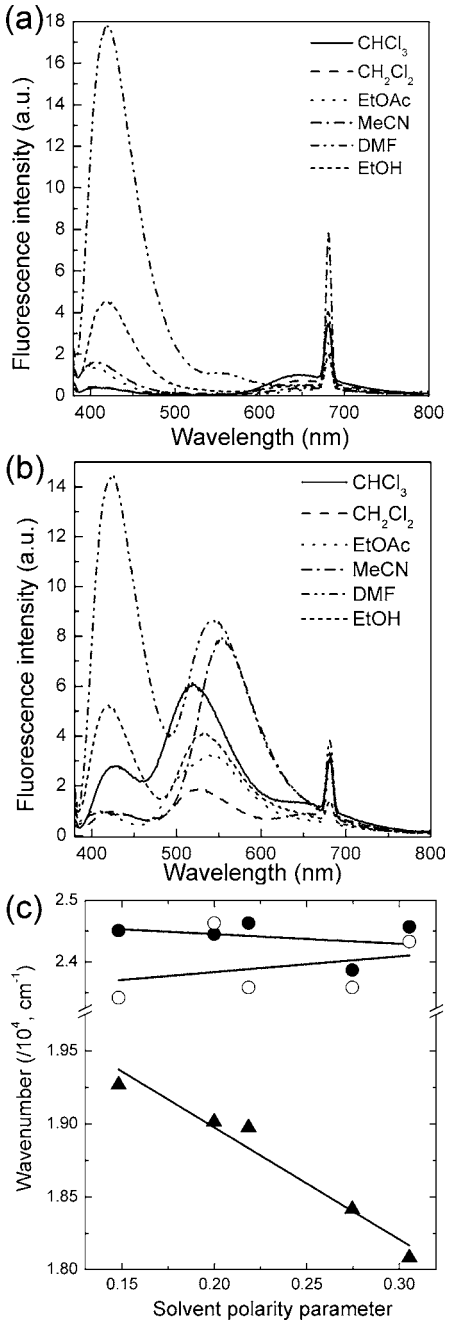

Figure 3. Measurements of fluorescence spectra of HNBO (a) and HNBO–DPA (b) with differing solvent polarities. (c) Lippert-Mataga plot constructed for enol fluorescence of HNBO (~420 nm; open circles) and HNBO–DPA (~420 nm; filled circles) and the new fluorescence band (~540 nm) of HNBO–DPA (filled triangles). Solvent polarity parameter (f) is defined by $f = (\varepsilon - 1)/(2\varepsilon + 1) - (n^2 - 1)/(2n^2 + 1)$, where ε and n are dielectric constant and refractive index of solvent, respectively. f values: $CHCl_3$, 0.1481; EtOAc, 0.1998; CH_2Cl_2, 0.2184; DMF, 0.2746; CH_3CN, 0.3055.

for HNBO (a 30-fold increase) and HNBO–DPA (a 42-fold increase), respectively. Figure 4b reveals that the increased fluorescence band (560 nm) of HNBO is neither enol (416 nm) nor keto fluorescence (650 nm) but identical to the fluorescence spectrum of HNBO–DPA (Figures 1b and 4d). A similar behavior was previously reported by Jen and co-workers for bis(2-hydroxyphenylbenzoxazole) fluorophores.[76] Since the base-induced optical responses are identical to those observed

dx.doi.org/10.1021/ic300476e | Inorg. Chem. 2012, 51, 8760–8774

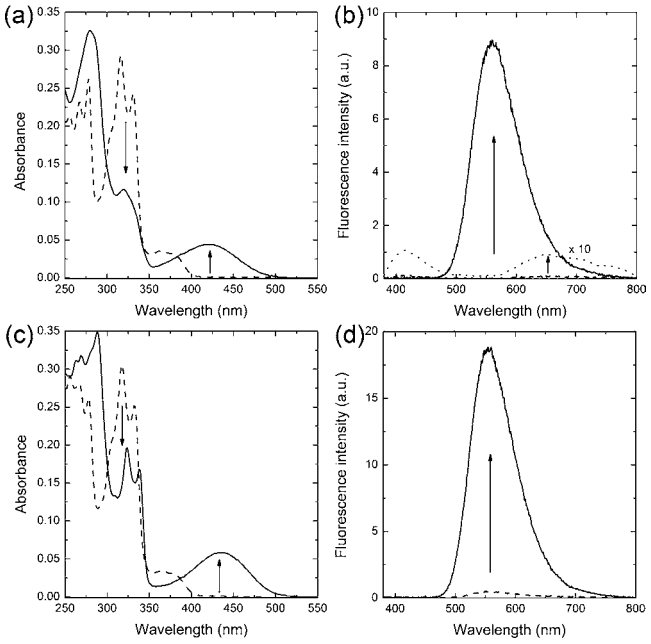

Figure 4. UV−vis absorption and photoluminescence spectral change of HNBO (a and b) and HNBO−DPA (c and d) upon the addition of base (aqueous sodium hydroxide, 50 equiv) to CH_3CN solutions containing either HNBO or HNBO−DPA (10 μM): (dashed lines) before the addition of base; (solid lines) after the addition of base. The dashed line in b is magnified by 10-fold (dotted line) to indicate enol and keto emission bands. Arrows indicate direction of spectral changes. A 340 nm excitation beam was provided to CH_3CN solutions.

for zinc complexation, the results provide strong evidence that zinc coordination provokes deprotonation of HNBO−DPA in solution state.

Transient Absorption and Electrochemical Measurements. To gain further information on the photophysical origin for the zinc response, we performed nanosecond and femtosecond laser flash photolysis experiments with Ar-saturated CH_3CN solutions containing HNBO−DPA in the absence and presence of zinc ions (O.D. = 0.1 at 355 and 420 nm for zinc-free and -bound forms, respectively). The transient absorption spectrum of the zinc-free form at 4 μs delay features distinct bands at 420, 470, and 700 nm under nanosecond laser excitation (Figure 5a). The 420 nm transient absorption band was previously assigned to be keto form for 2-(2′-hydroxyphenyl)benzoxazole (HBO).[77,78] We assign 470 and 700 nm absorption bands as radical anion of HNBO (i.e., $HNBO^{\bullet-}$) and radical cation of DPA (i.e., $DPA^{\bullet+}$), respectively. The radical cation of HNBO−DPA ($HNBO-DPA^{\bullet+}$) was independently generated by electron transfer from HNBO−DPA to the electron-transfer state of 9-mesityl-10-methylacridinium ion ($Acr^{\bullet}-Mes^{\bullet+}$), which was produced upon nanosecond laser excitation of $Acr^{+}-Mes$,[79−81] exhibiting the absorption bands at 460 and 700 nm (SI, Figure S2). The 470 nm absorption band due to $HNBO^{\bullet-}$ was also observed in the spectroelectrochemical measurements (SI, Figure S3) of HNBO (−2.2 V) and HNBO−DPA (−2.0 V). Interestingly, the absorption bands at 470 and 700 nm are long-lived with decay time constants of 38 μs (Figures 5c and d). Their identical decay time constants are indicative of an intramolecular radical ion pair. Addition of zinc ions quenches the transient absorption bands at 470 and 700 nm (delay time = 4 μs; Figure 5b), as expected for zinc-induced suppression of photoinduced electron transfer (PeT).

Femtosecond transient absorption spectra of a zinc-free form in Figure 5e show the conversion of the singlet excited state of HNBO (λ_{max} = 640 nm) to $DPA^{\bullet+}$ (λ_{max} ∼ 700 nm), which is also observed in nanosecond transient absorption spectrum (Figure 5a). The transient absorption at 470 nm due to $HNBO^{\bullet-}$ is not detected because of the limitation of the detection of absorption shorter than 490 nm. Addition of zinc ions suppresses formation of $DPA^{\bullet+}$ (λ_{max} = 700 nm) as shown in Figure 5f. Taken together, the results obtained by nanosecond and femtosecond laser flash photolysis reveal occurrence of intramolecular PeT from DPA to HNBO in the zinc-free state. Since PeT is generally considered to generate a nonemissive charge-separated state (CS; i.e., $HNBO^{\bullet-}-DPA^{\bullet+}$), suppression of PeT by zinc coordination is responsible for the fluorescence turn-on of HNBO−DPA.

Cyclic voltammograms shown in Figure 6 also suggest zinc-induced modulation in PeT. HNBO−DPA possesses peaks at 1.11 and 1.62 V (vs SCE) which correspond to oxidation of DPA and HNBO, respectively. These oxidation peaks are also observed in differential pulse voltammetry (SI, Figure S4). Inserting the experimental values (i.e., $E_+(DPA/DPA^{\bullet+})$ = 1.11 V; $E_-(HNBO/HNBO^{\bullet-})$ = −0.75 V (SI, Figure S5); ΔE_{00} = 3.59 eV) into the Rehm−Weller equation[82] yields a positive driving force for PeT ($-\Delta G_{PeT}$ = 1.73 eV).[83,84] Although the value of the driving force includes an experimental error of ±0.1 eV because the irreversible oxidation and reduction of HNBO−DPA, the PeT process is highly exergonic. As expected, addition of zinc ions (5 equiv) suppresses the oxidation of the free DPA moiety at 1.11 V (Figure 6), whereas only HNBO oxidation is observed before the solvent oxidation. An ability of DPA for a photoinduced electron donor is therefore lost by the zinc coordination, leading to the fluorescence turn-on.

DFT/TD-DFT Calculations. The steady-state and transient photophysical measurements and electrochemical characterizations establish the PeT mechanism for the zinc-induced fluorescence turn-on. To gain additional structural insight into the mechanism, DFT/TD-DFT calculations (B3LYP/6-31+G(d,p)//uB3LYP/6-31+G(d,p)) were carried out. TD-DFT calculations with uB3LYP/6-31+G(d,p) were previously employed to predict influence of zinc binding in fluorescent sensors.[85] Figure 7 depicts calculated geometry of neutral and deprotonated forms of HNBO and HNBO−DPA, and a deprotonated zinc complex of HNBO−DPA ($[Zn(HNBO-DPA)]^{+}$). Crystal structure geometry of $[Zn(HNBO-DPA)]^{2+}$ is shown for comparison. It should be noted that while the crystal structure of $[Zn(HNBO-DPA)]^{2+}$ maintains proton of naphthol, steady-state photophysical results strongly suggest deprotonation in solution state (vide supra).

Molecular orbitals participating in the lowest energy singlet transition are displayed, and electronic transitions calculated by TD-DFT methods are summarized in Table 2. Transition energies calculated for the singlet excited state (S_1) are 327 nm for neutral forms of HNBO and HNBO−DPA, but their transition characters are markedly different. The S_1 state of an enol form of HNBO is constructed by $\pi-\pi^*$ transition of the HNBO unit (L_HC), whereas a DPA-to-HNBO charge-transfer (L_DL_HCT) transition and an intramolecular charge-transfer (I_HCT) transition at the HNBO part are responsible for S_1 state of HNBO−DPA. Meanwhile, zinc coordination to HNBO−DPA ($[Zn(HNBO-DPA)]^{2+}$) suppresses this contribution of

dx.doi.org/10.1021/ic300476e | Inorg. Chem. 2012, 51, 8760−8774

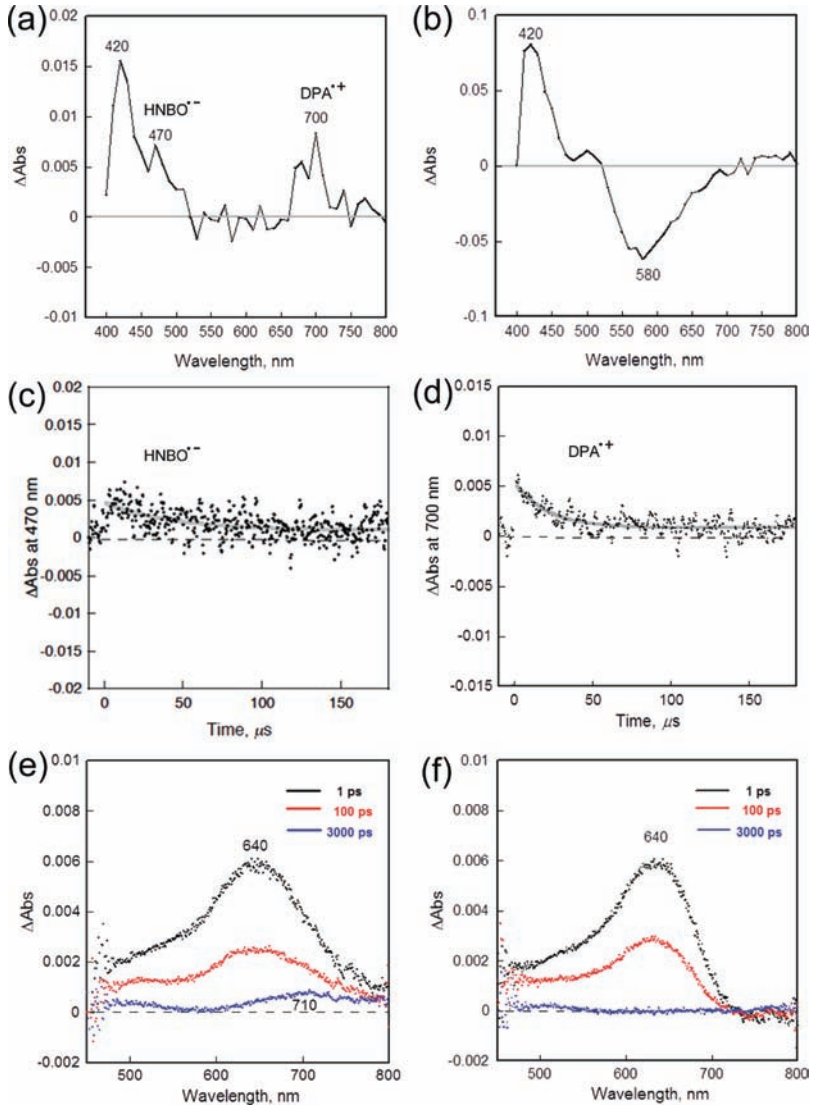

Figure 5. Transient absorption spectra of CH_3CN solutions containing HNBO−DPA measured at 4 μs after nanosecond laser excitation at λ_{ex} = 355 nm for the zinc-free form and λ_{ex} = 420 nm for the zinc-bound form in the absence (a) and presence (b) of zinc ions (5 equiv). Decay profiles of nanosecond transient absorption for the zinc-free form of HNBO−DPA recorded at 470 and 700 nm are shown in c and d, respectively. Gray lines are fit to a single exponential decay model: (c) τ = 38 μs; (d) τ = 38 μs. Transient absorption spectra of HNBO−DPA measured at 1, 100, and 3000 ps after femtosecond laser excitation at λ_{ex} = 356 nm in the absence (e) and presence (f) of zinc ion (5 equiv).

DPA (L_DL_HCT), resulting in π-orbitals of HNBO being dominant for the occupied orbital (HOMO). Thus, a significant difference in the transition character (i.e., a $\pi-\pi^*$ transition of the HNBO (L_HC) and a HNBO-to-DPA charge transfer transition (L_HL_DCT)) is identified for the singlet transition of $[Zn(HNBO-DPA)]^{2+}$. Despite the slight red shift compared to those (327 nm) of HNBO and HNBO−DPA, transition energy (388 nm) of $[Zn(HNBO-DPA)]^{2+}$ is still higher than that experimentally observed (Figure 1).

Deprotonation of naphthol destabilizes molecular orbitals, among which, HOMO occurring at naphtholate is preferentially affected (Figure 7). Corresponding S_1 state energy decreases in all cases: 553, 552, and 537 nm for deprotonated forms of HNBO ($HNBO^-$), HNBO−DPA ($HNBO-DPA^-$), and a zinc complex of HNBO−DPA ($[Zn(HNBO-DPA)]^+$), respectively. This prediction is in accordance with the observation for zinc- (Figure 1) and base-induced (Figure 4) spectral changes. In particular, the deprotonated species including $[Zn(HNBO-DPA)]^+$ possess a charge-transfer transition (i.e., intramolecular naphtholate to the whole HNBO unit charge-transfer transition, I_HCT) that may account for the distinguished solvatochromism (Figure 3c).

Fluorescence Turn-On Mechanism. Taking the results into account, the following conclusions can be drawn:

(1) A deprotonated form of HNBO, 2-(2′-benzoxazolyl)-3-naphtholate, is responsible for the fluorescence enhancement and the new band in the UV−vis absorption spectrum.
(2) Intramolecular PeT from DPA to HNBO occurs to generate a nonemissive charge-separated (CS) state.
(3) The deprotonation is facilitated by zinc coordination.
(4) The intramolecular PeT is suppressed by zinc coordination.

The most plausible mechanism that accounts for the zinc-induced fluorescence turn-on is depicted in Figure 8. In the absence of zinc, complete or partial photoinduced excited-state electron transfer from DPA to HNBO occurs to generate a

dx.doi.org/10.1021/ic300476e | Inorg. Chem. 2012, 51, 8760−8774

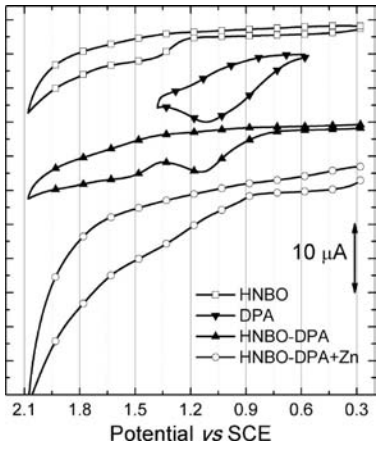

Figure 6. Cyclic voltammograms of HNBO, DPA, HNBO−DPA, and zinc complex of HNBO−DPA. Measurement conditions are described in the Experimental Section, and peak potentials are summarized in Table 1.

nonemissive charge-separated (CS) state. In contrast, zinc coordination to DPA suppresses the electron transfer to prohibit the generation of the CS state. At the same time, zinc coordination promotes deprotonation of the naphthol group. In deprotonated state, photoinduced electron transfer from DPA to HNBO becomes thermodynamically unfavorable due to decreased reduction potential of $HNBO^-$ (i.e., $-\Delta G_{PeT}(HNBO^- - DPA \rightarrow HNBO^{2-} - DPA^{\bullet+}) < 0$). Collectively, zinc binding effectively suppresses occurrence of PeT by combined influences of deprotonation (decreasing reduction potential of the electron acceptor, HNBO) and the coordination to DPA (increasing oxidation potential of the electron donor, DPA), leading to fluorescence turn-on.

Table 2. Summary of TD-DFT Calculation Results for Neutral and Deprotonated Forms of HNBO, HNBO−DPA, and Zinc Complex of HNBO−DPA

	state	transition energy (nm)	participating MO	transition character[a]
HNBO[b]	S_1	327 (0.7258)[c]	HOMO − 1 → LUMO (0.67)[d]	L_HC
$HNBO^-$ [b]	S_1	553 (0.1918)	HOMO → LUMO (0.71)	I_HCT
HNBO−DPA[b]	S_1	327 (0.6669)	HOMO − 2 → LUMO (0.67)	L_DL_HCT + I_HCT
HNBO−DPA^- [b]	S_1	552 (0.1273)	HOMO → LUMO (0.70)	I_HCT + L_HL_DCT
[Zn(HNBO−DPA)]$^{2+}$ [e]	S_1	388 (0.1291)	HOMO → LUMO + 1 (0.59)	L_HC + L_HL_DCT
[Zn(HNBO−DPA)]$^+$ [b]	S_1	537 (0.0028)	HOMO → LUMO (0.70)	L_HL_DCT
	S_2	490 (0.0262)	HOMO → LUMO + 2 (0.70)	I_HCT + L_HL_DCT
	S_3	387 (0.0127)	HOMO − 1 → LUMO (0.70)	L_HL_DCT

[a] L_HC (HNBO-centered $\pi-\pi^*$ transition), I_HCT (intramolecular charge-transfer transition of HNBO), L_DL_HCT (DPA-to-HNBO charge-transfer transition), and L_HL_DCT (HNBO-to-DPA charge-transfer transition). [b] Optimized geometry (B3LYP/6-31+G(d,p)). [c] Oscillator strength. [d] Expansion coefficient. [e] Crystal structure geometry.

Zinc Sensing in pH 7.0 Buffers. The zinc sensing capability of HNBO−DPA has been examined in pH 7.0 buffers (25 mM PIPES). UV−vis absorption spectrum of a buffer solution containing a zinc-bound form of HNBO−DPA

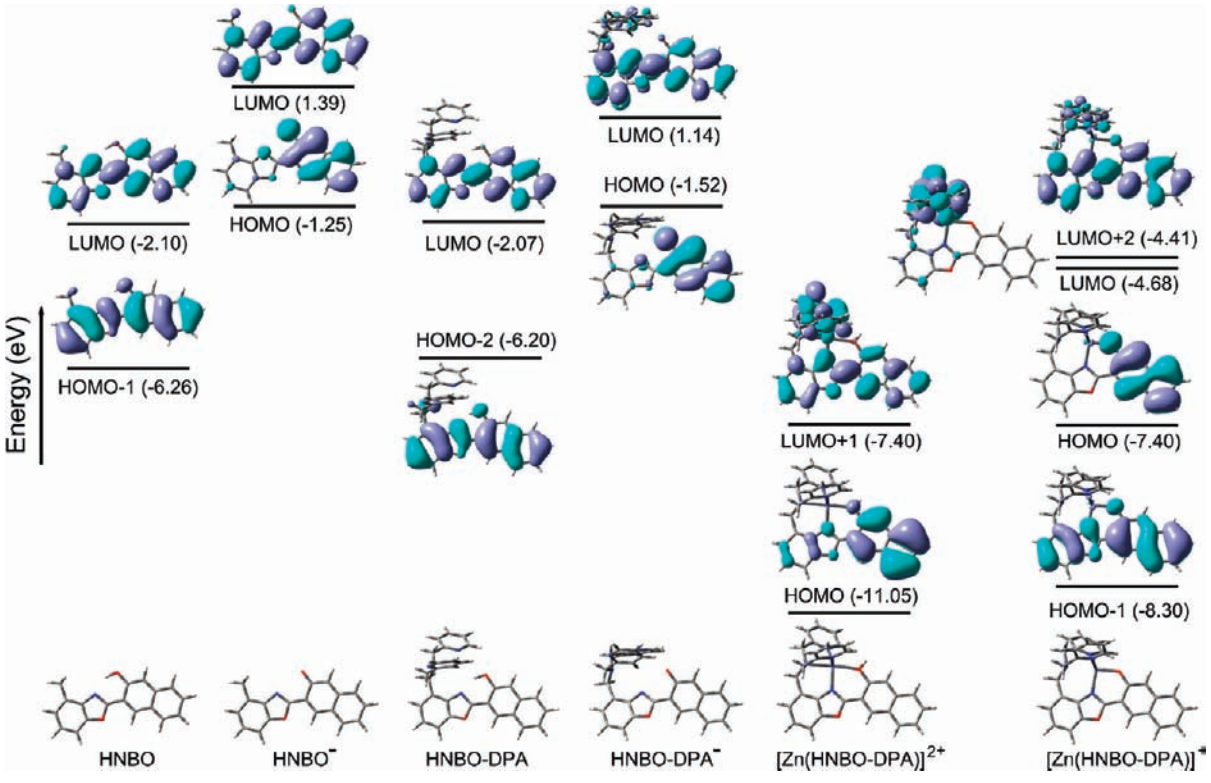

Figure 7. Isosurface (0.020 electron $bohr^{-3}$) of molecular orbitals participating in the lowest energy singlet states for the neutral and deprotonated forms for HNBO, HNBO−DPA, and a zinc complex of HNBO−DPA ($[Zn(HNBO-DPA)]^{2+}$).

dx.doi.org/10.1021/ic300476e | Inorg. Chem. 2012, 51, 8760−8774

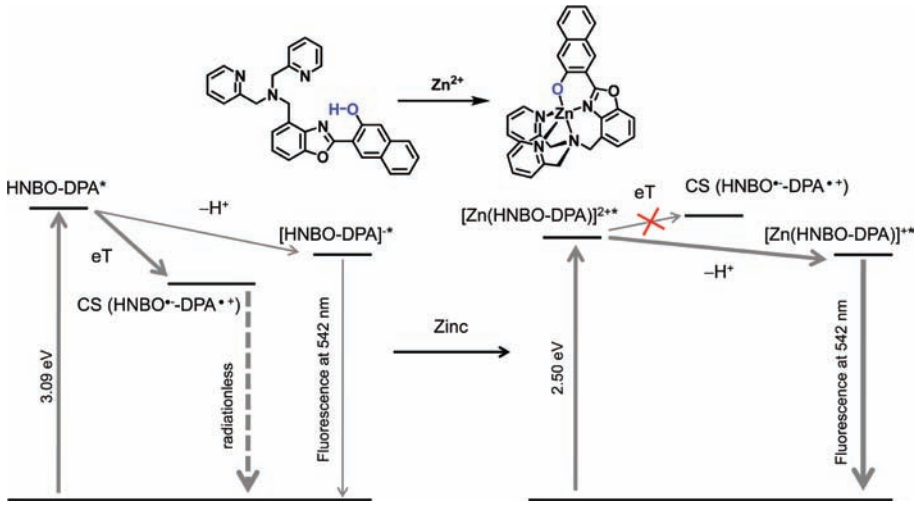

Figure 8. Proposed mechanism for the zinc-responsive fluorescence turn-on of HNBO–DPA: HNBO–DPA*, Franck–Condon excited state; CS (HNBO$^{\bullet-}$–DPA$^{\bullet+}$), an intramolecular charge-separated state; [Zn(HNBO–DPA)]$^{2+}$*, Franck–Condon excited state of zinc complex of HNBO–DPA; [Zn(HNBO–DPA)]$^{+}$*, an excited state of a deprotonated zinc complex of HNBO–DPA.

(10 μM, 1 equiv of $ZnCl_2$) is identical to that observed in CH_3CN (Figures 1a and 9a), which indicates zinc-induced deprotonation of naphthol. Response of the probe to zinc ions results in a 44-fold fluorescence increase without a spectral shift (Figure 9b; λ_{em} = 535 nm). A binding titration isotherm plotting integrated fluorescence intensity as a function of total zinc concentration reveals 1:1 binding (SI, Figure S6a). A Job's plot confirms this binding stoichiometry (SI, Figure S6b). A dissociation constant (K_d) for zinc binding was determined by employing zinc-buffered solutions (100 mM HEPES, 100 mM $NaNO_3$, 10 mM HEDTA, and 0.59–10 mM total $ZnCl_2$; pH 7.4). Using a mathematical model for a 1:1 equilibrium,[86] a K_d value was determined to be 12 pM (Figure 9c). Such a tight zinc binding property can be rationalized by the pentacoordinate chelate structure (Figure 2). Validity of the K_d value was further assessed by a fluorescence competitive assay. In this study, HNBO–DPA (0–5 equiv) was continuously added to a pH 7.0 buffer solution (25 mM PIPES) containing $ZnCl_2$ (2 equiv) and a fluorescence turn-on zinc sensor, Zinpyr-1 (ZP1), which was established by Lippard and co-workers (10 μM).[87] The solution containing probes was excited at 500 nm where HNBO–DPA and its zinc complex do not absorb but ZP1 and its complex do. K_d values of ZP1 were previously determined to be 0.04 pM and 1.2 nM (Scheme 2).[88] Since the zinc dissociation constant of HNBO–DPA is 12 pM, free HNBO–DPA can take out a more weakly bound zinc ion (K_d = 1.2 nM) that is coordinated to ZP1. As expected, addition of HNBO–DPA to the mixture decreases the fluorescence intensity of a zinc complex of ZP1, but the fluorescence intensity of the mixture was not restored to that of a zinc-free form of ZP1 (Figure 9d) because a more tightly bound zinc ion (K_d = 0.04 pM) is still bound to ZP1. The fluorescent limit of detection of HNBO–DPA for zinc is 2.3 pM as determined by the three sigma method.

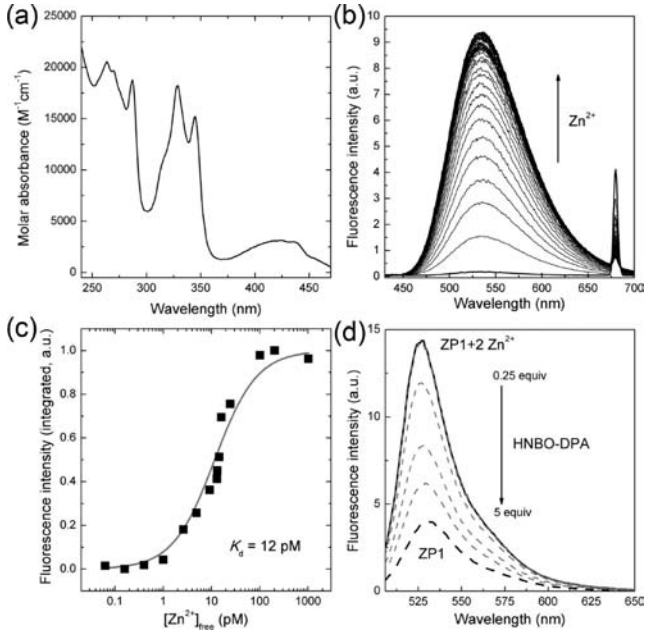

Figure 9. (a) UV–vis absorption spectrum of HNBO–DPA (10 μM) in the presence of $ZnCl_2$ (1 equiv). (b) Fluorescence spectral change (λ_{ex} = 340 nm) of HNBO–DPA with the continuous addition of $ZnCl_2$ (0–2 equiv). (c) A titration isotherm plotting fluorescence intensity of HNBO–DPA as a function of free zinc concentration. Zinc-buffered solutions of pH = 7.4 were used for measurements. (d) Fluorescence competitive assay (λ_{ex} = 500 nm) of a zinc complex of ZP1 solution (10 μM; $[ZnCl_2]_{added}/[ZP1]$ = 2) by the addition of HNBO–DPA (0–5 equiv). pH 7.0 buffer solutions (25 mM PIPES) were used for measurements except c.

Most interestingly, the fluorescent zinc sensing ability of HNBO–DPA is not affected by pH changes between 3 and 10 (Figure 10a). The huge fluorescence turn-on is conserved in buffer solutions at various pH (Figure 10b; pH 7.0, 100 mM PIPES; pH 8.0, 100 mM HEPES (*N*-(2-hydroxyethyl)-piperazine-*N*′-(2-ethanesulfonic acid)); pH 9.5, 100 mM CHES (2-(cyclohexylamino)ethanesulfonic acid); pH 11, 100 mM CAPS (3-(cyclohexylamino)-1-propanesulfonic acid)). Since prominent proton-induced fluorescence turn-on is typically observed for fluorescent sensors relying on PeT, lack of the proton-induced interferences of HNBO–DPA is of great importance. This favorable feature is, however, in contrast to the case observed in acetonitrile (Figures 4b and d). According to the photophysical mechanism (Figure 8), deprotonation of

dx.doi.org/10.1021/ic300476e | Inorg. Chem. 2012, 51, 8760–8774

Scheme 2. Fluorescence Competitive Assay of HNBO−DPA

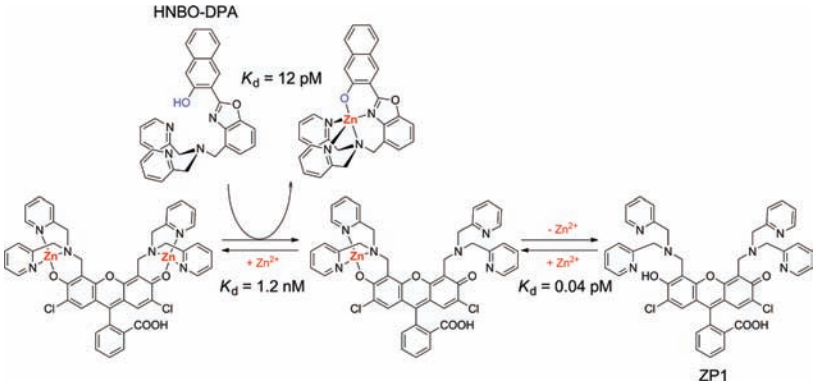

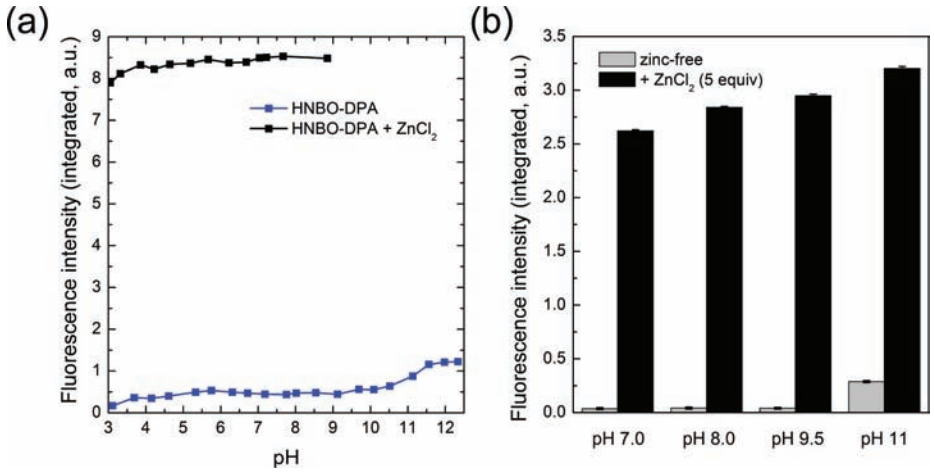

Figure 10. (a) pH titration of HNBO−DPA and its zinc complex. A 10 μM portion of HNBO−DPA was dissolved in milli-Q water containing 100 mM KCl, and pH was adjusted by using KOH and HCl standard solutions. (b) Fluorescence zinc (5 equiv) response of HNBO−DPA (10 μM) in buffered solutions: pH 7.0, 100 mM PIPES; pH 8.0, 100 mM HEPES; pH 9.5, 100 mM CHES; pH 11, 100 mM CAPS.

Scheme 3. pH Effect on the Fluorescence of HNBO−DPA

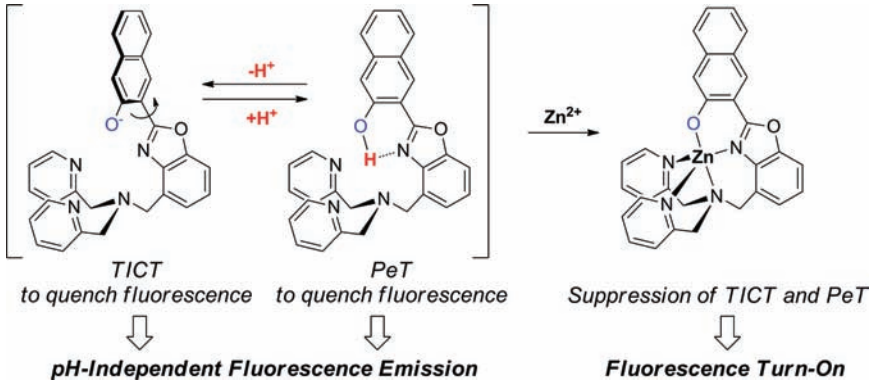

HNBO moiety should produce fluorescence turn-on, which is clearly not the case for aqueous solutions.

These considerations lead us to suggest that PeT is not solely responsible for the fluorescent zinc response in aqueous solutions. It is speculated that nonradiative twisted intramolecular charge transfer (TICT) occurs in the deprotonated form. TICT deactivation of fluorescence emission was observed in protic solvents for deprotonated form of ESIPT-active 2-(2′-hydroxyphenyl)benzimidazole[89] and its derivatives.[90] In addition, TICT is supported by our DFT and TD-DFT calculations which predict dihedral distortion for the deprotonated state of HNBO−DPA (SI, Figure S7). By contrast, TICT would be completely prohibited in the zinc-bound form. The observation that neither protonation to DPA (at low pH) nor deprotonation of naphthol (at high pH) affects fluorescence intensity of HNBO−DPA indicates the minimized proton interference. That is, fluorescence of the deprotonated species is quenched by TICT at high pH, while nonradiative PeT occurs to quench the emission at low pH. The overall effect is weak fluorescence emission over the wide pH range (Scheme 3). This is in sharp contrast to the zinc case, wherein zinc

dx.doi.org/10.1021/ic300476e | Inorg. Chem. 2012, 51, 8760−8774

coordination suppresses PeT and TICT, producing bright fluorescence emission.

HNBO−DPA shows exclusive fluorescence response to zinc ions among biologically relevant metal ions (Figure 11); Na^+, Mg^{2+}, K^+, Ca^{2+}, Mn^{2+}, Co^{2+}, and Ni^{2+} ions do not interfere the fluorescent zinc response. To our surprise, the sensor discriminates zinc ions in the presence of tightly binding transition metal ions. Actually, HNBO−DPA exhibits fluorescent zinc response over divalent Cu^{2+}, Fe^{2+}, Cd^{2+}, and Hg^{2+} ions, which are known to bind stronger than zinc according to the Irving−Williams series. The pentacoordinated chelate disposition of HNBO−DPA may account for the improved zinc selectivity (Figure 2).

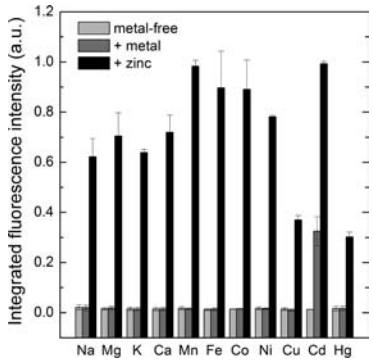

Figure 11. Fluorescent zinc ion selectivity of HNBO−DPA (10 μM): light gray bar, fluorescence intensity of the zinc-free form; gray bar, fluorescence intensity in the presence of metal ion (Na^+, Mg^{2+}, K^+, Ca^{2+} ions, 100 equiv; other metal ions, 1 equiv to HNBO−DPA); black bar, fluorescence intensity after subsequent addition of zinc ion (1 equiv) to the mixture. pH 7.0 buffer solutions (25 mM PIPES) were used for measurements.

Fluorescent Detection of Intracellular Zinc Ions. We have shown above the ability of HNBO−DPA in detecting zinc ions. To evaluate in vivo zinc bioimaging utilities, HNBO−DPA (5 μM) was incubated with live A549 (human lung carcinoma) and HeLa (human cervix adenocarcinoma) cells that were supplied with exogenous zinc ions (5 μM) by means of sodium pyrithione as a zinc carrier. It is found that while cells incubated with HNBO−DPA alone display very weak background fluorescence, zinc-treated cells exhibit strong fluorescence (Figure 12). As expected for a zinc-responsive sensor, incubation with a membrane-permeable zinc ion chelator, TPEN (*N*,*N*,*N*′,*N*′-tetrakis(2-picolyl)ethylenediamine),[91] reduces fluorescence intensity, indicating that the fluorescence signals are consequence of the response to intracellular zinc ions. The results obtained from cell experiments show that HNBO−DPA is cell-permeable and can monitor intracellular zinc ions effectively.

Encouraged by the fluorescent imaging of intracellular zinc ions, HNBO−DPA was applied to monitor intact zinc ions released from cells that undergo apoptosis. It has been known that free zinc ions are released from intracellular metalloproteins during apoptosis and can be detected with fluorescent probes for zinc ions.[20,92,93] A549 and HeLa cells were exposed to H_2O_2 (100 μM)[20] or apoptozole (10 μM)[94] for 24 h, which are known to induce apoptosis, and subsequently incubated with HNBO−DPA for 1 h. The results of microscopic analysis show typical morphology of apoptotic cells (SI, Figure S8)[95] and display bright fluorescence signals

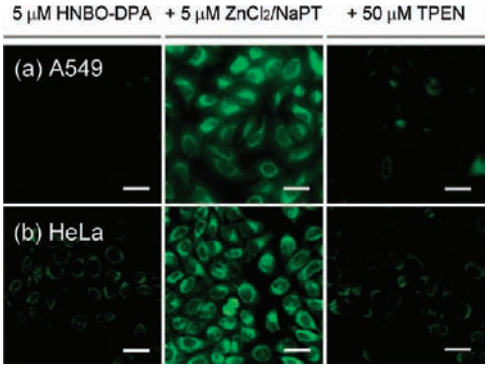

Figure 12. Detection of zinc ions in live mammalian cells with HNBO−DPA. Fluorescence microscope images of A549 (a) and HeLa (b) cells. Cells were incubated with 5 μM HNBO−DPA for 1 h in the absence (left) and presence (middle) of 5 μM $ZnCl_2$/sodium pyrithione. Cells pretreated with 50 μM TPEN were incubated with 5 μM HNBO−DPA and 5 μM $ZnCl_2$/sodium pyrithione (right). Scale bars = 25 μm.

(Figure 13). To confirm that fluorescence turn-on was due to response of HNBO−DPA to released zinc ions, cells exposed to H_2O_2 (100 μM) or apoptozole (10 μM) for 24 h were treated with TPEN (50 μM) for 1 h before treatment with the probe. Indeed, TPEN remarkably attenuates the bright HNBO−DPA fluorescence (Figure 13), indicating that the probe detects free zinc ions released during apoptosis.

Fluorescent Detection of Endogenous Zinc Ions in Zebrafish. Zebrafish have been widely used as an animal model to demonstrate detection of a variety of biological ions and molecules using fluorescent probes due to permeability to exogenously supplied compounds and suitability to fluorescence microscopy.[41,94,96−100] We therefore employed HNBO−DPA to trace the distribution of endogenous zinc ions in live zebrafish. Zebrafish embryos were incubated with 5 μM HNBO−DPA at various time points during early development. At 18 h post fertilization (hpf) of the embryo, a green-spotted band was seen in the bottom of the venter (Figure 14a).[41,101] During development, the necklace-like green-spotted band was brighter and moved to the top of the venter until 48 hpf (Figures 14b and c). After 60 hpf, scattered bright spots were distributed around the pericardial sac (Figures 14d and e). However, the treatment of 48 h-old zebrafish with 100 μM TPEN resulted in the disappearance of the green spots (yellow boxes in Figures 14f and g), suggesting that the green fluorescent band may result from endogenous zinc pools in fish. This observation is quite similar with results obtained previously.[41,101] Abnormal developmental defects were not observed in zebrafish treated with HNBO−DPA, showing that the zinc probe is biologically orthogonal. Results obtained from animal studies demonstrate the usefulness of HNBO−DPA for detecting biologically relevant ions in living organisms.

III. EXPERIMENTAL SECTION

Materials and Synthesis. Materials obtained from commercial suppliers were used without further purification unless otherwise stated. All glassware, syringes, magnetic stirring bars, and needles were thoroughly dried in a convection oven. Reactions were monitored using thin layer chromatography (TLC) with commercial TLC plates (silica gel 60 F_{254}, Merck Co.). Silica gel column chromatography was performed with silica gel 60 (particle size 0.063−0.200 mm, Merck Co.). ^1H and ^{13}C NMR spectra were recorded on a Bruker Avance 300 spectrometer. High resolution mass spectra were acquired by

dx.doi.org/10.1021/ic300476e | Inorg. Chem. 2012, 51, 8760−8774

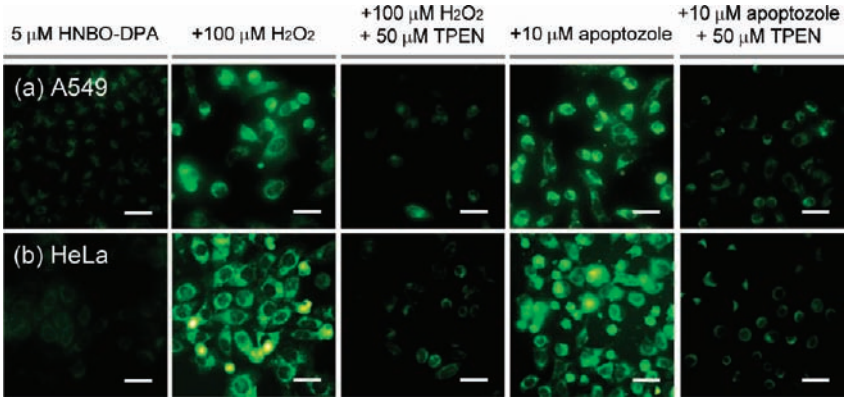

Figure 13. Detection of endogenous zinc ions released during apoptosis using HNBO–DPA. Fluorescence microscope images of A549 (a) and HeLa (b) cells. Cells were exposed to 100 μM H_2O_2 or 10 μM apoptozole for 24 h to induce apoptosis. Then, cells were incubated with 5 μM HNBO–DPA for visualization. Cells were additionally treated with 50 μM TPEN to confirm specific zinc response of HNBO–DPA. Scale bars = 25 μm.

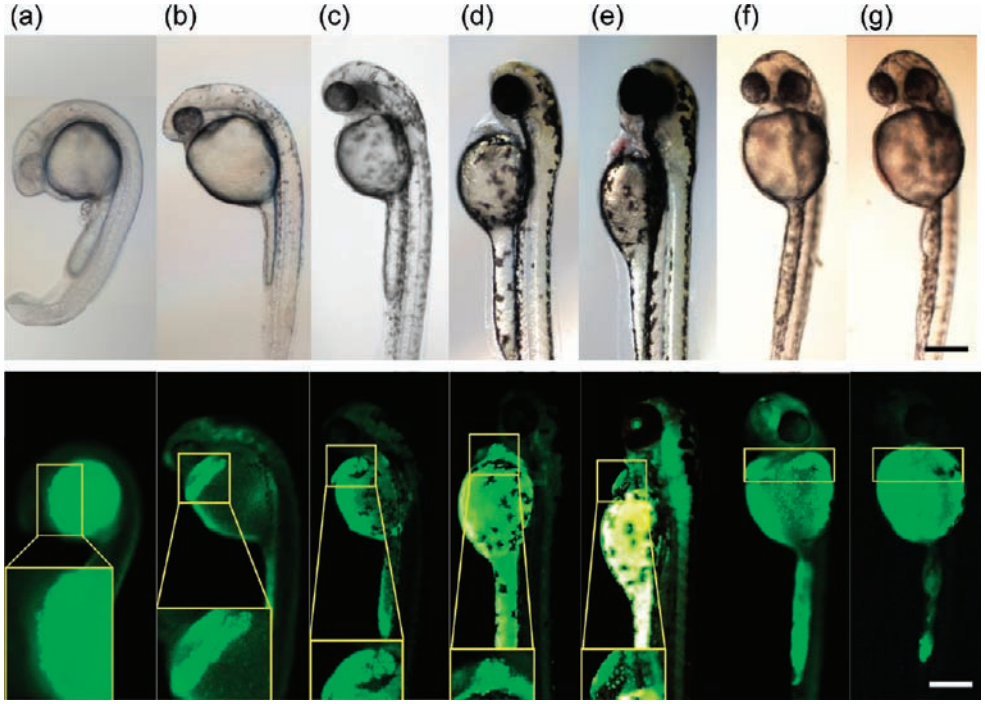

Figure 14. Detection of endogenous zinc ions in zebrafish with HNBO–DPA. Fluorescence microscope images of (a) 18, (b) 24, (c) 48, (d) 60, and (e) 72 h-old zebrafish incubated with HNBO–DPA for 1 h: (top panels) bright field images; (bottom panels) fluorescence microscope images. Yellow boxes show magnified images. Fluorescence microscope images of 48 h-old zebrafish incubated with HNBO–DPA for 1 h in the absence (f) and presence (g) of 100 μM TPEN. Scale bar = 250 μm.

employing a JEOL JMS-600W/JMS-700GC and an Applied Biosystems Tempo nano HPLC/QSTAR Elite spectrometers. Elemental analyses were performed on a CE Instrument EA1110 instrument. ZP1 was prepared according to the established method.[87]

2-(2′-Hydroxy-3′-naphthyl)-4-methylbenzoxazole (HNBO, 3). 3-Hydroxy-2-naphthoic acid (2.00 g, 10.6 mmol) and 2-amino-*m*-cresol (1.31 g, 10.6 mmol) were suspended in polyphosphoric acid (10.0 g) and heated overnight at 160 °C. The reaction mixture was cooled to room temperature and poured onto 300 mL of water. After neutralization, the mixture was filtered and washed with water. Silica gel column purification with ethyl acetate:*n*-hexane (1:50, v/v) and subsequent recrystallization in ethyl acetate gave 1.04 g of orange needles (35%). ^{1}H NMR (300 MHz, $CDCl_3$) δ: 2.66 (s, 3H), 7.20 (d, 1H, J = 3.8 Hz), 7.28–7.37 (m, 2H), 7.45–7.51 (m, 3H), 7.72 (d, 1H, J = 4.1 Hz), 7.87 (d, 1H, J = 4.1 Hz), 8.61 (s, 1H), 11.39 (s, 1H). ^{13}C NMR (75 MHz, $CDCl_3$) δ: 16.7, 108.2, 111.8, 113.0, 124.2, 125.8, 125.9, 126.7, 127.7, 128.6, 128.7, 128.9, 130.4, 136.8, 139.6, 149.3, 154.5, 162.0. HRMS (EI, positive) calcd for $C_{18}H_{13}NO_2$ (M^+), 275.0946; found, 275.0944. Anal. calcd for $C_{18}H_{13}NO_2$: C, 78.53; H, 4.76; N, 5.09. Found: C, 78.51; H, 4.74; N, 5.11.

2-(2′-Methoxymethyloxy-3′-naphthyl)-4-methylbenzoxazole (4). Chloromethyl methyl ether (2.1 mL, 27 mmol) was added to a CH_2Cl_2 solution (100 mL) containing **3** (1.0 g, 3.6 mmol) and diisopropylethylamine (4.7 mL, 27 mmol) at 0 °C. The mixture was refluxed overnight. Water was poured into the solution and the product was recovered with CH_2Cl_2 (100 mL, three times). The extracted organic layer was dried over anhydrous $MgSO_4$ and evaporated to afford 0.95 g of the desired product (82%). ^{1}H NMR (300 MHz, $CDCl_3$) δ: 2.72 (s, 3H), 3.61 (s, 3H), 5.44 (s, 2H), 7.17 (d, 1H, J = 3.8 Hz), 7.27 (t, 1H, J = 7.8 Hz), 7.40–7.46 (m, 2H), 7.53 (t, 1H, J = 7.9 Hz), 7.57 (s, 1H), 7.79 (d, 1H, J = 4.1 Hz), 7.90 (d, 1H, J = 3.8 Hz), 8.62 (s, 1H). ^{13}C NMR (75 MHz, $CDCl_3$) δ: 16.9, 56.7, 95.6,

dx.doi.org/10.1021/ic300476e | Inorg. Chem. 2012, 51, 8760–8774

108.1, 111.9, 119.1, 125.0, 125.1, 125.2, 127.1, 128.3, 128.8, 129.0, 131.0, 132.7, 135.7, 141.5, 150.9, 152.9, 161.3. HRMS (ESI, positive) calcd for $C_{20}H_{18}NO_3$ ([M + H]$^+$), 320.1287; found, 320.1277.

4-Bromomethyl-2-(2′-methoxymethyloxy-3′-naphthyl)-benzoxazole (5). A CCl_4 solution (100 mL) of **4** (0.94 g, 2.9 mmol), *N*-bromosuccinimide (0.53 g, 2.9 mmol), and azobisisobutyronitrile (0.024 g, 0.15 mmol) was refluxed overnight under an Ar atmosphere. The reaction mixture was cooled to 0 °C and resulting precipitates were removed by filtration. The filtrate was concentrated under vacuum and reprecipitated in methanol (100 mL) to afford 0.84 g of white powder (72%). ^{1}H NMR (300 MHz, $CDCl_3$) δ: 3.63 (s, 3H), 4.99 (s, 2H), 5.45 (s, 2H), 7.36 (t, 1H, J = 7.5 Hz), 7.38−7.46 (m, 2H), 7.52−7.58 (m, 3H), 7.79 (d, 1H, J = 4.1 Hz), 7.92 (d, 1H, J = 4.0 Hz), 8.67 (s, 1H). ^{13}C NMR (75 MHz, $CDCl_3$) δ: 28.0, 56.8, 95.7, 111.0, 112.0, 118.6, 125.3, 125.5, 127.1, 128.5, 128.8, 129.0, 130.0, 133.0, 135.9, 141.0, 151.1, 152.9, 162.3. HRMS (ESI, positive) calcd for $C_{20}H_{17}BrNO_3$ ([M + H]$^+$), 398.0392; found, 398.0391.

4-(Di(2-picolyl)aminomethyl)-2-(2′-methoxymethyloxy-3′-naphthyl)benzoxazole (6). A THF solution (100 mL) of **5** (0.84 g, 2.1 mmol), di(2-picolyl)amine (1.2 mL, 6.4 mmol), and Na_2CO_3 (2.2 g, 21 mmol) was stirred overnight at room temperature. The reaction mixture was concentrated under vacuum and poured into water. The organic compounds were extracted with CH_2Cl_2 (100 mL, three times), which was dried over anhydrous $MgSO_4$ and concentrated. Silica gel column purification with CH_2Cl_2:methanol (12:1, v/v) gave 0.79 g of yellowish oil (72%). ^{1}H NMR (300 MHz, $CDCl_3$) δ: 3.58 (s, 3H), 3.96 (s, 4H), 4.26 (s, 2H), 5.43 (s, 2H), 7.13 (t, 2H, J = 5.7 Hz), 7.34−7.46 (m, 2H), 7.50−7.59 (m, 4H), 7.66 (td, 2H, J = 7.8, 0.8 Hz), 7.74−7.80 (m, 3H), 7.91 (d, 1H, J = 4.1 Hz), 8.52 (d, 2H, J = 2.2 Hz), 8.64 (s, 1H). ^{13}C NMR (75 MHz, $CDCl_3$) δ: 53.5, 56.7, 60.5, 95.6, 109.3, 111.9, 119.0, 122.1, 123.0, 124.7, 125.1, 125.2, 127.1, 128.3, 128.7, 129.0, 131.3, 132.7, 135.8, 136.6, 141.7, 149.2, 151.0, 153.0, 160.3, 161.6. HRMS (ESI, positive) calcd for $C_{32}H_{29}N_4O_3$ ([M + H]$^+$), 517.2240; found, 517.2238.

4-(Di(2-picolyl)aminomethyl)-2-(2′-hydroxy-3′-naphthyl)-benzoxazole (HNBO−DPA, 7). **6** (0.79 g, 1.5 mmol) and *p*-toluenesulfonic acid monohydrate (1.3 g, 6.7 mmol) were dissolved in methanol (100 mL) and stirred overnight at room temperature. The reaction mixture was concentrated under vacuum and then poured into water. The solution was neutralized by K_2CO_3. The organic compounds were extracted with CH_2Cl_2 (100 mL, three times), dried over anhydrous $MgSO_4$, and concentrated. Silica gel column purification with CH_2Cl_2:methanol (12:1, v/v) gave 0.35 g of white powder (49%). ^{1}H NMR (300 MHz, $CDCl_3$) δ: 3.91 (s, 4H), 4.16 (s, 2H), 7.15 (t, 2H, J = 5.7 Hz), 7.34−7.42 (m, 2H), 7.47−7.57 (m, 4H), 7.65−7.76 (m, 5H), 7.89 (d, 1H, J = 4.2 Hz), 8.53 (d, 2H, J = 2.4 Hz), 8.64 (s, 1H), 11.27 (s, 1H). ^{13}C NMR (75 MHz, $CDCl_3$) δ: 53.9, 60.5, 109.6, 111.8, 112.9, 122.2, 123.0, 124.2, 125.8, 126.2, 126.7, 127.7, 128.6, 128.8, 128.9, 130.7, 136.8, 136.9, 139.7, 149.3, 149.5, 154.5, 159.8, 162.4. HRMS (FAB, positive) calcd for $C_{30}H_{25}N_4O_2$ ([M + H]$^+$), 473.1978; found, 473.1982. Anal. calcd for $C_{30}H_{24}N_4O_2$: C, 76.25; H, 5.12; N, 11.86. Found: C, 76.24; H, 5.12; N, 11.85.

X-ray Crystallography. A single crystal of [Zn(HNBO−DPA)]-$(ClO_4)_2$·CH_3CN was picked from an CH_3CN solution and mounted on a goniometer head. Data collections were carried out on a Bruker SMART AXS diffractometer equipped with a monochromator in the Mo Kα (λ = 0.71073 Å) incident beam. The CCD data were integrated and scaled using a Bruker-SAINT software package, and the structure was solved and refined using SHEXTL V 6.12.[102] All non-hydrogen atoms were refined with anisotropic thermal parameters. Hydrogen atoms were located in the calculated positions except for H33, which was found from the Fourier difference map. Crystal data for [Zn(HNBO−DPA)]$(ClO_4)_2$·CH_3CN: $C_{32}H_{27}Cl_2N_5O_{10}Zn$, Monoclinic, $P2(1)/c$, Z = 4, a = 10.9325(2), b = 16.4960(3), c = 18.1446(3) Å, β = 107.2770(10)°, V = 3124.60(10) Å^3, μ = 1.027 mm^{-1}, ρ_{calcd} = 1.654 g/cm^3, R_1 = 0.0296, wR_2 = 0.1069, GOF = 0.951 for 7180 unique reflections and 456 variables. The crystallographic data for [Zn(HNBO−DPA)]$(ClO_4)_2$·CH_3CN are listed in Table S1 of the Supporting Information, and Table S2 of the Supporting Information lists the selected bond distances and angles. CCDC-831430 for [Zn(HNBO−DPA)]$(ClO_4)_2$·CH_3CN contains the supplementary crystallographic data for this paper. These data can be obtained free of charge via www.ccdc.cam.ac.uk/data_request/cif (or from the Cambridge Crystallographic Data Centre, 12, Union Road, Cambridge CB2 1EZ, UK; fax (+44) 1223−336−033 or deposit@ccdc.cam.ac.uk).

Spectroscopic Measurements. Milli-Q grade water (18.2 MΩ·cm) was used to prepare solutions for spectroscopic measurements. PIPES (piperazine-*N*,*N*′-bis(2-ethanesulfonic acid), ≥99%) was purchased from Aldrich. A pH 7.0 buffer solution was prepared by dissolving PIPES (25 mM) in milli-Q water and adjusting the pH with a standard KOH solution (45 wt %, Aldrich) or an HCl solution (1 N, Aldrich). The buffer solution was further treated with Chelex100 resin (BIO-RAD) to remove trace metal ions and filtered through a membrane (pore size = 0.45 μm). pH of the buffer solution was reexamined before use. Fresh metal stock solutions (typically, 0.1 or 0.01 M) were prepared in milli-Q water using the corresponding chloride salts: NaCl (≥99.5%, Aldrich), KCl (puratonic grade, Calbiochem), $MgCl_2$ (99.99%, Aldrich), $CaCl_2$ (99.99%, Aldrich), $MnCl_2$ (99.99%, Aldrich), $FeCl_2$ (99.99%, Aldrich), $CoCl_2$ (99.9%, Aldrich), $NiCl_2$ (99.99%, Aldrich), $ZnCl_2$ (99.999%, Aldrich), $CuCl_2$ (99.999%, Aldrich), $CdCl_2$ (99.999%, Aldrich), and $HgCl_2$ (99.999%, Aldrich). A TPEN solution was prepared by dissolving *N*,*N*,*N*′,*N*′-tetrakis(2-picolyl)ethylenediamine (≥99%, Sigma) in DMSO (99.9%, Aldrich). $Zn(ClO_4)_2$·$6H_2O$ (Aldrich) was dissolved in CH_3CN (spectrophotometric grade, Aldrich) to 1 mM and 10 mM concentration. The sensor for aqueous solutions was dissolved in DMSO to a concentration of 10 mM. The sensor solution was partitioned into Eppendorf centrifuge tubes and stored frozen. For spectroscopic measurements, the sensor solution was thawed just before experiments. Typically, 3 mL of pH 7.0 PIPES buffer and 3 μL of the sensor solution (10 mM) were mixed to give a 10 μM solution. CH_3CN solutions (spectrophotometric grade, Aldrich) of the sensor (10 μM) were freshly prepared before measurements. A 1 cm × 1 cm fluorimeter cell (Hellma) was used for steady-state optical measurements. UV−vis absorption spectra were collected on a Varian Cary 50 spectrophotometer and a Shimadzu UV-1650PC spectrophotometer at room temperature. Fluorescence spectra were obtained by using a Varian Cary Eclipse fluorescence spectrophotometer and a Quanta Master 40 scanning spectrofluorimeter at room temperature. The solutions were excited by using an excitation beam at 340 nm throughout fluorescence measurements unless otherwise indicated. A 3 μL portion of a 1 mM $ZnCl_2$ or $Zn(ClO_4)_2$ solution was added per each titration step. pH titrations of fluorescence intensity were conducted with KOH solutions (milli-Q water, pH = 12) containing KCl (100 mM) and the sensor (10 μM) by the addition of aqueous HCl solutions (6, 2, 1, 0.5, 0.1, or 0.05 M). The photoluminescence quantum yield (Φ_{Fl}) was determined through an absolute method by employing an integrated sphere. Ar-saturated CH_3CN solutions containing HNBO−DPA (125 μM) with or without zinc ion (2 equiv) were excited by a 420 nm beam and the total emission was collected for integration. All solutions for photoluminescence measurements were air-equilibrated except those for measurements of photoluminescence quantum yields, photoluminescence lifetimes, and femtosecond and nanosecond transient absorption. Photoluminescence lifetime measurements were performed by a Photon Technology International GL-3300 with a Photon Technology International GL-302, nitrogen laser/pumped dye laser system equipped with a four channel digital delay/pulse generator (Stanford Research System Inc. DG535) and a motor driver (Photon Technology International MD-5020). Excitation wavelength was 430 nm using dimethyl-POPOP (Exciton Co., USA) as a laser dye. The laser pulse of 337 nm was focused at CH_3CN solutions of HNBO−DPA (O.D. = 0.2 at 345 nm) in the absence or presence of zinc ion (2 equiv).

Determination of K_d. Zinc-buffered solutions (pH 7.4; 100 mM HEPES, 100 mM $NaNO_3$, and 10 mM HEDTA) were employed to determine a dissociation constant (K_d). The procedure reported by Nagano and co-workers was modified to prepare 15 solutions of free zinc concentrations varied from 6.3 fM to 1.0 nM.[86] A 3 μL sensor solution (10 mM, DMSO) was added to each zinc-buffered solution (3

dx.doi.org/10.1021/ic300476e | Inorg. Chem. 2012, 51, 8760−8774

mL) and kept at least for 3 h. The fluorescence spectrum of the solution was recorded, and the intensity was calculated by integrating the spectrum from 430 to 700 nm. A zinc binding titration isotherm plotting fluorescence intensity was constructed as a function of free zinc concentration, which was fitted to a 1:1 binding equation.[86]

Femtosecond Laser Flash Photolysis. Femtosecond transient absorption spectroscopy experiments were conducted using an ultrafast source, Integra-C (Quantronix Corp.), an optical parametric amplifier, TOPAS (Light Conversion Ltd.), and a commercially available optical detection system, Helios provided by Ultrafast Systems LLC. The source for the pump and probe pulses were derived from the fundamental output of Integra-C (780 nm, 2 mJ/pulse, and fwhm =130 fs) at a repetition rate of 1 kHz. Here, 75% of the fundamental output of the laser beam was introduced into TOPAS which has optical frequency mixers resulting in tunable range from 285 to 1660 nm, while the rest of the output was used for white light generation. Prior to generating the probe continuum, a variable neutral density filter was inserted in the path in order to generate stable continuum, then the laser pulse was fed to a delay line that provides an experimental time window of 3.2 ns with a maximum step resolution of 7 fs. An excitation wavelength at 356 nm of TOPAS output, which are fourth harmonic of signal or idler pulses, was chosen as the pump beam. As this TOPAS output consists of not only desirable wavelength but also unnecessary wavelengths, the latter was deflected using a wedge prism with wedge angle of 18°. The desirable beam was irradiated at the sample cell with a spot size of 1 mm diameter where it was merged with the white probe pulse in a close angle (<10°). The probe beam after passing through a 2 mm sample cell was focused on a fiber optic cable, which was connected to a CCD spectrograph for recording the time-resolved spectra (470−800 nm). Typically, 3000 excitation pulses were averaged for 3 s to obtain the transient spectrum at a set delay time. Kinetic traces at appropriate wavelengths were assembled from the time-resolved spectral data. All measurements were conducted at 295 K.

Nanosecond Laser Flash Photolysis. Ar-saturated CH_3CN solutions were excited by Nd:YAG laser (Continuum, SLII-10; 4−6 ns fwhm) at 355 nm with 5 mJ/pulse. Time courses of the transient absorption were measured by an InGaAs-PIN photodiode (Hamamatsu 2949) as a detector. The output from the photodiodes and a photomultiplier tube was recorded with a digitized oscilloscope (Tektronix, TDS3032; 300 MHz). All experiments were performed at 298 K.

Electrochemical Measurements. Cyclic voltammetry experiments were carried out with a CHI630 B instrument (CH Instruments, Inc.) using three electrode cell assemblies. Pt wires were used for working and counter electrodes. An $Ag/AgNO_3$ couple was employed as a reference electrode. Measurements were carried out in Ar-saturated CH_3CN (3 mL) with tetra-*n*-butylammonium hexafluorophosphate (Bu_4NPF_6) as a supporting electrolyte (0.1 M) at a scan rate of 100 mV/s. The sensor concentration was 1 mM. A ferrocenium/ferrocene reference was employed. For spectroelectrochemical measurements, an Ar-saturated CH_3CN solution containing either HNBO or HNBO−DPA (1 mM) and Bu_4NPF_6 (0.1 M) was delivered to a 1 cm × 0.5 mm quartz cuvette in which a Pt mesh working electrode was integrated. A Pt wire and an $Ag/AgNO_3$ couple were employed for a counterelectrode and a reference electrode, respectively. UV−vis absorption spectra were recorded under a negative bias (−2.2 V for HNBO and −2.0 V for HNBO−DPA).

Calculations. Quantum chemical calculations based on density functional theory (DFT) were carried out using a Gaussian 09 program.[103] Ground state geometry optimization and single point calculations were performed using the B3LYP functional and the 6-31+G(d,p) basis set. Additional B3LYP calculations with the cc-pVTZ basis set were performed, and the results were essentially the same (not shown). Structures of neutral forms were optimized and frequency calculations were performed to examine stability of the optimized geometries. The resulting geometries were used as starting geometries for optimization of deprotonated forms. Geometry of the zinc-bound HNBO−DPA was extracted from its crystal structure and used without further optimization. For TD-DFT calculations, the unrestricted uB3LYP functional and the identical basis set used for the geometry optimization were applied. Twenty lowest singlet states were calculated and analyzed.

Detection of Zinc Ions in Live Mammalian Cells with HNBO−DPA. A549 (human lung carcinoma) and HeLa cells (human cervix adenocarcinoma) were seeded in a 24-well plate at a density of 2×10^3 cells per well in culture media (RPMI-1640 supplemented with 10% fetal bovine serum). After 24 h, 5 μM HNBO−DPA in the culture media containing 0.1 vol % DMSO was added to the cells, and the cells were incubated for 1 h at 37 °C. After washing twice with 400 μL of Dulbecco's phosphate buffered saline (DPBS, without calcium and magnesium) to remove the remaining probe, the cells were further treated with 5 μM $ZnCl_2$/sodium pyrithione in culture media for 0.5 h. The treated cells were imaged by a fluorescence microscope (Eclipse TE2000-S, Nikon, Japan). For TPEN experiments, 5 μM HNBO−DPA in the culture media containing 0.1 vol % DMSO was added to the cells, and the cells were incubated for 1 h at 37 °C. After washing twice with DPBS, the cells were treated with 50 μM TPEN for 0.5 h, washed with DPBS, and then treated with 5 μM $ZnCl_2$/sodium pyrithione in culture media. The treated cells were imaged by a fluorescence microscope.

To induce apoptosis, A549 and HeLa cells were treated with 100 μM H_2O_2 or 10 μM apoptozole in the culture media for 24 h at 37 °C. The cells were incubated with 5 μM HNBO−DPA in the culture media for 1 h at 37 °C. After washing twice with DPBS, the cells were imaged by a fluorescence microscope. For TPEN experiments, cells treated with 100 μM H_2O_2 or 10 μM apoptozole were incubated with 50 μM TPEN for 1 h. After washing twice with DPBS, 5 μM HNBO−DPA in the culture media was added to the cells, and the cells were incubated for 1 h at 37 °C. Finally the treated cells were rinsed and imaged by a fluorescence microscope.

Tracing Distribution of Zinc Ions in Zebrafish with HNBO−DPA. Zebrafish were kept at 28 °C and maintained at optimal breeding conditions.[100] For mating, male and female zebrafish were maintained in one tank at 28 °C on a 12-h light/12-h dark cycle, and then, the spawning of eggs was triggered by giving light stimulation in the morning. Almost all eggs were fertilized immediately. All stages of zebrafish were maintained in E3 embryo media (15 mM NaCl, 0.5 mM KCl, 1 mM $MgSO_4$, 1 mM $CaCl_2$, 0.15 mM KH_2PO_4, 0.05 mM Na_2HPO_4, 0.7 mM $NaHCO_3$, and 5−10% methylene blue; pH 7.5). Zebrafish embryos at 18, 24, 48, 60, and 72 hpf were incubated with 5 μM HNBO−DPA in E3 media containing 0.1 vol % DMSO for 1 h at 28 °C. Alternatively, 48 h-old zebrafish were exposed to 100 μM TPEN in E3 media containing 0.1 vol % DMSO for 1 h at 28 °C. After washing with E3 media to remove the remaining TPEN, the zebrafish were further incubated with 5 μM HNBO−DPA in E3 media for 1 h at 28 °C. The treated zebrafish were imaged by a fluorescence microscope.

IV. SUMMARY

We have developed a novel fluorescent zinc sensor (HNBO−DPA) by conjugating an ESIPT chromophore, 2-(2′-hydroxy-3′-naphthyl)benzoxazole (HNBO), and a zinc-specific di(2-picolyl)amine (DPA) receptor through a methylene bridge. Addition of zinc ions induces a strong fluorescence turn-on without a spectral shift, which is not explained by the typical ESIPT scheme. The fluorescence of HNBO−DPA is neither ESIPT keto emission nor normal enol emission. Fluorescence measurements performed under basic conditions establish that zinc coordination promotes deprotonation of the ESIPT group. Nanosecond and femtosecond laser flash photolysis measurements for HNBO−DPA identify zinc-modulated photoinduced electron transfer (PeT). Cyclic voltammetry experiments further evidence occurrence of PeT, and positive driving force ($-\Delta G_{PeT}$ = 1.73 eV) is calculated by the Rehm−Weller equation. The fluorescence turn-on mechanism is therefore suppression of PeT, which is strongly supported by DFT/TD-DFT calculations. In pH 7.0 buffers, the probe displays a 44-

dx.doi.org/10.1021/ic300476e | Inorg. Chem. 2012, 51, 8760−8774

fold fluorescence turn-on in response to zinc ions with a K_d of 12 pM, which has been further examined by a fluorescence competitive assay. The fluorescence response of the probe to zinc ions is conserved over a broad range of pH due to the unique fluorescence response mechanism of the probe. The probe is able to detect zinc ions among biologically relevant metal ions, with particular selectivity to zinc over divalent transition metal ions. In addition, intracellular zinc ions have been successfully monitored in live mammalian cells. The zinc sensing utility has been further extended to visualization of endogenous zinc ions released from cells that undergo apoptosis. Furthermore, HNBO−DPA allows for tracing endogenous zinc-rich pools of zebrafish embryos during the early development. The work described herein reports the unique fluorescence zinc response of the ESIPT-based sensor. The novel photophysical mechanism has been established and its bioimaging utility is proved to be excellent for the detection of endogenous zinc ions.

■ ASSOCIATED CONTENT

Ⓢ Supporting Information

Complete ref 103, spectroelectrochemical results for HNBO and HNBO−DPA, zinc binding isotherms, Job's plot, cyclic voltammograms, DFT-calculated geometry, the limit of detection value, and intracellular zinc imaging results. This material is available free of charge via the Internet at http://pubs.acs.org.

■ AUTHOR INFORMATION

Corresponding Author

*E-mail: odds2@ewha.ac.kr (Y.Y.); fukuzumi@chem.eng.osaka-u.ac.jp (S.F.); injae@yonsei.ac.kr (I.S.); parksy@snu.ac.kr (S.Y.P.); wwnam@ewha.ac.kr (W.N.).

Author Contributions

⊥These authors contributed equally to this work.

Notes

The authors declare no competing financial interest.

■ ACKNOWLEDGMENTS

This work was supported by CRI (W.N., S.Y.P., I.S.), GRL (2010-00353) (W.N.), and WCU program (R31-2008-000-10010-0 and R32-2008-000-10217-0) (W.N., I.S.) from the National Research Foundation (NRF) of Korea, Grants-in-Aid (Nos. 20108010 and 23750014) a Global COE program (S.F.), "the Global Education and Research Center for Bio-Environmental Chemistry" from the Japan Society of Promotion of Science, and RP-Grant 2009 (Y.Y.) of Ewha Womans University. Y.Y. acknowledges Prof. Joan S. Valentine at Ewha Womans University for helpful comments and suggestions.

■ REFERENCES

(1) Lipscomb, W. N.; Strater, N. *Chem. Rev.* **1996**, *96*, 2375−2433.
(2) Frederickson, C. J.; Koh, J. Y.; Bush, A. I. *Nat. Rev. Neurosci.* **2005**, *6*, 449−462.
(3) Burdette, S. C.; Lippard, S. J. *Proc. Natl. Acad. Sci. U.S.A.* **2003**, *100*, 3605−3610.
(4) Berg, J. M.; Shi, Y. *Science* **1996**, *271*, 1081−1085.
(5) O'Halloran, T. V. *Science* **1993**, *261*, 715−725.
(6) Outten, C. E.; Tobin, D. A.; Penner-Hahn, J. E.; O'Halloran, T. V. *Biochemistry* **2001**, *40*, 10417−10423.
(7) Finney, L. A.; O'Halloran, T. V. *Science* **2003**, *300*, 931−936.
(8) Outten, C. E.; O'Halloran, T. V. *Science* **2001**, *292*, 2488−2492.
(9) Dunn, M. F. *Biometals* **2005**, *18*, 295−303.
(10) Redenti, S.; Ripps, H.; Chappell, R. L. *Exp. Eye Res.* **2007**, *85*, 580−584.
(11) Galasso, S. L.; Dyck, R. H. *Mol. Med.* **2007**, *13*, 380−387.
(12) Costello, L. C.; Franklin, R. B. *Mol. Cancer* **2006**, *5*, 17−29.
(13) Takeda, A. *Biometals* **2001**, *14*, 343−351.
(14) Que, E. L.; Domaille, D. W.; Chang, C. J. *Chem. Rev.* **2008**, *108*, 1517−1549.
(15) Cuajungco, M. P.; Lees, G. J. *Neurobiol. Dis.* **1997**, *4*, 137−169.
(16) Bush, A. I.; Pettingell, W. H.; Multhaup, G.; Paradis, M. D.; Vonsattel, J. P.; Gusella, J. F.; Beyreuther, K.; Masters, C. L.; Tanzi, R. E. *Science* **1994**, *265*, 1464−1467.
(17) Koh, J.-Y.; Suh, S. W.; Gwag, B. J.; He, Y. Y.; Hsu, C. Y.; Choi, D. W. *Science* **1996**, *272*, 1013−1016.
(18) Truong-Tran, A. Q.; Carter, J.; Ruffin, R. E.; Zalewski, P. D. *Biometals* **2001**, *14*, 315−330.
(19) Zalewski, P. D.; Forbes, I. J.; Seamark, R. F.; Borlinghaus, R.; Betts, W. H.; Lincoln, S. F.; Ward, A. D. *Chem. Biol.* **1994**, *1*, 153−161.
(20) Kimura, E.; Aoki, S.; Kikuta, E.; Koike, T. *Proc. Natl. Acad. Sci. U.S.A.* **2003**, *100*, 3731−3736.
(21) Xu, Z.; Yoon, J.; Spring, D. R. *Chem. Soc. Rev.* **2010**, *39*, 1996−2006.
(22) Carol, P.; Sreejith, S.; Ajayaghosh, A. *Chem. Asian J.* **2007**, *2*, 338−348.
(23) Domaille, D. W.; Que, E. L.; Chang, C. J. *Nat. Chem. Biol.* **2008**, *4*, 168−175.
(24) Dai, Z.; Canary, J. W. *New J. Chem.* **2007**, *31*, 1708−1718.
(25) Jiang, P.; Guo, Z. *Coord. Chem. Rev.* **2004**, *248*, 205−229.
(26) Tomat, E.; Lippard, S. J. *Curr. Opin. Chem. Biol.* **2010**, *14*, 225−230.
(27) Linert, W.; Jameson, G. N. L.; Jameson, R. F.; Jellinger, K. A. *Met. Ions Life Sci.* **2006**, *1*, 281−320.
(28) Kimura, E.; Koike, T. *Chem. Soc. Rev.* **1998**, *27*, 179−184.
(29) Lim, N. C.; Freake, H. C.; Bruckner, C. *Chem.—Eur. J.* **2005**, *11*, 38−49.
(30) Frederickson, C. J.; Kasarskis, E. J.; Ringo, D.; Frederickson, R. E. *J. Neurosci. Methods* **1987**, *20*, 91−103.
(31) Nolan, E. M.; Lippard, S. J. *Acc. Chem. Res.* **2009**, *42*, 193−203.
(32) Wong, B. A.; Friedle, S.; Lippard, S. J. *Inorg. Chem.* **2009**, *48*, 7009−7011.
(33) Zhang, X.-a.; Hayes, D.; Smith, S. J.; Friedle, S.; Lippard, S. J. *J. Am. Chem. Soc.* **2008**, *130*, 15788−15789.
(34) Goldsmith, C. R.; Lippard, S. J. *Inorg. Chem.* **2006**, *45*, 555−561.
(35) Nolan, E. M.; Jaworski, J.; Racine, M. E.; Sheng, M.; Lippard, S. J. *Inorg. Chem.* **2006**, *45*, 9748−9757.
(36) Nolan, E. M.; Lippard, S. J. *Inorg. Chem.* **2004**, *43*, 8310−8317.
(37) Komatsu, K.; Kikuchi, K.; Kojima, H.; Urano, Y.; Nagano, T. *J. Am. Chem. Soc.* **2005**, *127*, 10197−10204.
(38) Nolan, E. M.; Ryu, J. W.; Jaworski, J.; Feazell, R. P.; Sheng, M.; Lippard, S. J. *J. Am. Chem. Soc.* **2006**, *128*, 15517−15528.
(39) Urano, Y.; Tanaka, K.; Nagano, T.; Ohkubo, K.; Fukuzumi, S. *J. Am. Chem. Soc.* **2003**, *125*, 8666−8671.
(40) Ueno, T.; Urano, Y.; Setsukinai, K.; Takakusa, H.; Kojima, H.; Kikuchi, K.; Ohkubo, K.; Fukuzumi, S.; Nagano, T. *J. Am. Chem. Soc.* **2004**, *126*, 14079−14085.
(41) Qian, F.; Zhang, C.; Zhang, Y.; He, W.; Gao, X.; Hu, P.; Guo, Z. *J. Am. Chem. Soc.* **2009**, *131*, 1460−1468.
(42) Hanaoka, K.; Muramatsu, Y.; Urano, Y.; Terai, T.; Nagano, T. *Chem.—Eur. J.* **2010**, *16*, 568−572.
(43) Aoki, S.; Kagata, D.; Shiro, M.; Takeda, K.; Kimura, E. *J. Am. Chem. Soc.* **2004**, *126*, 13377−13390.
(44) Vinkenborg, J. L.; Nicolson, T. J.; Bellomo, E. A.; Koay, M. S.; Rutter, G. A.; Merkx, M. *Nat. Methods* **2009**, *6*, 737−740.
(45) Pina, J.; Seixas de Melo, J.; Pina, F.; Lodeiro, C.; Lima, J. C.; Parola, A. J.; Soriano, C.; Clares, M. P.; Albelda, M. T.; Aucejo, R. *Inorg. Chem.* **2005**, *44*, 7449−7458.
(46) Dick, B.; Ernsting, N. P. *J. Phys. Chem.* **1987**, *91*, 4261−4265.
(47) Goodman, J.; Brus, L. E. *J. Am. Chem. Soc.* **1978**, *100*, 7472−7474.

(48) Abou-Zied, O. K.; Jimenez, R.; Thompson, E. H. Z.; Millar, D. P.; Romesberg, F. E. *J. Phys. Chem. A* **2002**, *106*, 3665−3672.
(49) Iijima, T.; Momotake, A.; Shinohara, Y.; Sato, T.; Nishimura, Y.; Arai, T. *J. Phys. Chem. A* **2010**, *114*, 1603−1609.
(50) Rios Vazquez, S.; Rios Rodriguez, M. C.; Mosquera, M.; Rodriguez-Prieto, F. *J. Phys. Chem. A* **2008**, *112*, 376−387.
(51) Roshal, A. D.; Grigorovich, A. V.; Doroshenko, A. O.; Pivovarenko, V. G.; Demchenko, A. P. *J. Photochem. Photobiol. A Chem.* **1999**, *127*, 89−100.
(52) Singh, N.; Kaur, N.; Mulrooney, R. C.; Callan, J. F. *Tetrahedron Lett.* **2008**, *49*, 6690−6692.
(53) Tanaka, K.; Kumagai, T.; Aoki, H.; Deguchi, M.; Iwata, S. *J. Org. Chem.* **2001**, *66*, 7328−7333.
(54) Wu, K.-C.; Lin, Y.-S.; Yeh, Y.-S.; Chen, C.-Y.; Ahmed, M. O.; Chou, P.-T.; Hon, Y.-S. *Tetrahedron* **2004**, *60*, 11861−11868.
(55) Zhang, X. B.; Cheng, G.; Zhang, W.-J.; Shen, G.-L.; Yu, R.-Q. *Talanta* **2007**, *71*, 171−177.
(56) Henary, M. M.; Wu, Y.; Fahrni, C. J. *Chem.—Eur. J.* **2004**, *10*, 3015−3025.
(57) Henary, M. M.; Fahrni, C. J. *J. Phys. Chem. A* **2002**, *106*, 5210−5220.
(58) Taki, M.; Wolford, J. L.; O'Halloran, T. V. *J. Am. Chem. Soc.* **2003**, *126*, 712−713.
(59) Hindo, S. S.; Mancino, A. M.; Braymer, J. J.; Liu, Y.; Vivekanandan, S.; Ramamoorthy, A.; Lim, M. H. *J. Am. Chem. Soc.* **2009**, *131*, 16663−16665.
(60) Arslan, P.; Di virgilio, F.; Beltrame, M.; Tsien, R. Y.; Pozzan, T. *J. Biol. Chem.* **1985**, *260*, 2719−2727.
(61) Burdette, S. C.; Frederickson, C. J.; Bu, W.; Lippard, S. J. *J. Am. Chem. Soc.* **2003**, *125*, 1778−1787.
(62) Komatsu, K.; Kikuchi, K.; Kojima, H.; Urano, Y.; Nagano, T. *J. Am. Chem. Soc.* **2005**, *127*, 10197−10204.
(63) Xu, Y.; Pang, Y. *Chem. Commun.* **2010**, *46*, 4070−4072.
(64) Xu, Y.-Q.; Pang, Y. *Dalton Trans.* **2011**, *40*, 1503−1509.
(65) Helal, A.; Kim, H.-S. *Tetrahedron Lett.* **2009**, *50*, 5510−5515.
(66) Helal, A.; Lee, S. H.; Kim, S. H.; Kim, H.-S. *Tetrahedron Lett.* **2010**, *51*, 3531−3535.
(67) Helal, A.; Kim, S. H.; Kim, H.-S. *Tetrahedron* **2010**, *66*, 9925−9932.
(68) Yang, C.-C.; Tian, Y.; Chen, C.-Y.; Jen, A. K. Y.; Chen, W.-C. *Macromol. Rapid Commun.* **2007**, *28*, 894−899.
(69) Ma, Q.-J.; Zhang, X.-B.; Zhao, X.-H.; Gong, Y.-J.; Tang, J.; Shen, G.-L.; Yu, R.-Q. *Spectrochim. Acta A* **2009**, *73*, 687−693.
(70) Ohshima, A.; Momotake, A.; Arai, T. *Tetrahedron Lett.* **2004**, *45*, 9377−9381.
(71) Roy, P.; Dhara, K.; Manassero, M.; Banerjee, P. *Inorg. Chim. Acta* **2009**, *362*, 2927−2932.
(72) Roh, S.-G.; Kim, Y.-H.; Seo, K. D.; Lee, D. H.; Kim, H. K.; Park, Y.-I.; Park, J.-W.; Lee, J.-H. *Adv. Funct. Mater.* **2009**, *19*, 1663−1671.
(73) Yu, G.; Yin, S.; Liu, Y.; Shuai, Z.; Zhu, D. *J. Am. Chem. Soc.* **2003**, *125*, 14816−14824.
(74) Xu, H.; Xu, Z.-F.; Yue, Z.-Y.; Yan, P.-F.; Wang, B.; Jia, L.-W.; Li, G.-M.; Sun, W.-B.; Zhang, J.-W. *J. Phys. Chem. C* **2008**, *112*, 15517−15525.
(75) Seo, J.; Kim, S.; Park, S. Y. *J. Am. Chem. Soc.* **2004**, *126*, 11154−11155.
(76) Tian, Y.; Chen, C.-Y.; Yang, C.-C.; Young, A. C.; Jang, S.-H.; Chen, W.-C.; Jen, A. K. Y. *Chem. Mater.* **2008**, *20*, 1977−1987.
(77) Stephan, J. S.; Grellmann, K. H. *J. Phys. Chem.* **1995**, *99*, 10066−10068.
(78) Iijima, T.; Momotake, A.; Shinohara, Y.; Sato, T.; Nishimura, Y.; Arai, T. *J. Phys. Chem. A* **2010**, *114*, 1603−1609.
(79) Fukuzumi, S.; Kotani, H.; Ohkubo, K.; Ogo, S.; Tkachenko, N. V.; Lemmetyinen, H. *J. Am. Chem. Soc.* **2004**, *126*, 1600−1601.
(80) Ohkubo, K.; Kotani, H.; Fukuzumi, S. *Chem. Commun.* **2005**, 4520−4522.
(81) Fukuzumi, S.; Kotani, H.; Ohkubo, K. *Phys. Chem. Chem. Phys.* **2008**, *10*, 5159−5162.
(82) The electrostatic term (work term for the radical ion pair) is neglected in a highly polar solvent (MeCN).
(83) Kennedy, D. P.; Kormos, C. M.; Burdette, S. C. *J. Am. Chem. Soc.* **2009**, *131*, 8578−8586.
(84) Miura, T.; Urano, Y.; Tanaka, K.; Nagano, T.; Ohkubo, K.; Fukuzumi, S. *J. Am. Chem. Soc.* **2003**, *125*, 8666−8671.
(85) Hudson, G. A.; Cheng, L.; Yu, J.; Yan, Y.; Dyer, D. J.; McCarroll, M. E.; Wang, L. *J. Phys. Chem. B* **2010**, *114*, 870−876.
(86) Komatsu, K.; Urano, Y.; Kojima, H.; Nagano, T. *J. Am. Chem. Soc.* **2007**, *129*, 13447−13454.
(87) Walkup, G. K.; Burdette, S. C.; Lippard, S. J.; Tsien, R. Y. *J. Am. Chem. Soc.* **2000**, *122*, 5644−5645.
(88) Wong, B. A.; Friedle, S.; Lippard, S. J. *J. Am. Chem. Soc.* **2009**, *131*, 7142−7152.
(89) Brenlla, A.; Veiga, M.; Ríos Rodríguez, M. C.; Mosquera, M.; Rodríguez-Prieto, F. *Photochem. Photobiol. Sci.* **2011**, *10*, 1622−1636.
(90) Ríos Vázquez, S.; Ríos Rodriguez, M. C.; Mosquera, M.; Rodríguez-Prieto, F. *J. Phys. Chem. A* **2007**, *111*, 1814−1826.
(91) Nasir, M. S.; Fahrni, C. J.; Suhy, D. A.; Kolodsick, K. J.; Singer, C. P.; O'Halloran, T. V. *J. Biol. Inorg. Chem.* **1999**, *4*, 775−783.
(92) Zalewski, P. D.; Forbes, I. J.; Betts, W. H. *Biochem. J.* **1993**, *296*, 403−408.
(93) Zalewski, P. D.; Forbes, I. J.; Seamark, R. F.; Borlinghaus, R.; Betts, W. H.; Lincoln, S. F.; Ward, A. D. *Chem. Biol.* **1994**, *1*, 153−161.
(94) Williams, D. R.; Ko, S.-K.; Park, S.; Lee, M.-R.; Shin, I. *Angew. Chem., Int. Ed.* **2008**, *47*, 7466−7469.
(95) Kimura, E.; Aoki, S.; Kikuta, E.; Koike, T. *Proc. Natl. Acad. Sci. USA* **2003**, *100*, 3731−3735.
(96) Ikeda, K.; Kajiwara, K.; Tanabe, E.; Tokumaru, S.; Kishida, E.; Masuzawa, Y.; Kojo, S. *Biochem. Pharmacol.* **1999**, *57*, 1361−1365.
(97) Santra, M.; Ryu, D.; Chatterjee, A.; Ko, S.-K.; Shin, I.; Ahn, K. H. *Chem. Commun.* **2009**, 2115−2117.
(98) Ko, S.-K.; Chen, X.; Yoon, J.; Shin, I. *Chem. Soc. Rev.* **2011**, *40*, 2120−2130.
(99) Ko, S.-K.; Yang, Y.-K.; Tae, J.; Shin, I. *J. Am. Chem. Soc.* **2006**, *128*, 14150−14155.
(100) Yang, Y.-K.; Ko, S.-K.; Shin, I.; Tae, J. *Nat. Protocols* **2007**, *2*, 1740−1745.
(101) Xu, Z.; Baek, K.-H.; Kim, H. N.; Cui, J.; Qian, X.; Spring, D. R.; Shin, I.; Yoon, J. *J. Am. Chem. Soc.* **2010**, *132*, 601−610.
(102) Sheldrick, G. M. *SHELXTL/PC*, version 6.12 for Windows XP ed.; Bruker AXS Inc.: Madison, WI, 2001.
(103) Frisch, M. J.; et al. *Gaussian 09*, revision A.02; Gaussian, Inc.: Wallingford CT, 2009.